SAND2011-0059P

Finite Element Analysis of Tilt Behavior During the First Eugenie 1 Re-entry

Courtney G. Herrick and Dwayne Kicker
Sandia National Laboratories
4100 National Parks Highways
Carlsbad, NM 88220

1 Introduction

As a first step toward finding a way to mitigate or even eliminate the possibility of collapse of the brine cavern at the I&W site, the State of New Mexico and the City of Carlsbad in consultation with RESPEC Consulting and Services have attempted to determine the size and location of the cavity created by dissolution of an estimated six million cubic feet of salt. One proposed method was to re-enter the cavity through Eugenie 1 and perform a sonar survey. During the first re-entry attempt of Eugenie 1 on July 9-10 it was noted that the tiltmeters responded directly to the decrease in cavern pressure as the brine was allowed to flow out. In a manner similar to a beam deflecting under the application of a uniform stress, deformation on the surface above the cavern is believed to respond to the cavern's pressure change acting on its roof's span. The larger the span, the greater the deflection will be with changing pressure. Our thought is that by analyzing the behavior of the strata above a modeled cavern as its internal pressure is dropped, mimicking the events of the re-entry, the calculated changes in surface tilts could be used to constrain the size of the cavern when compared to the measured values. After investigating several analytical models, simplified finite element modeling was undertaken.

A schematic of the model concept is shown below in Figure 1. The model consists of four layers of material which represent the geologic strata at the I&W facility. In the third layer, which represents the salt section, is a cavern which extends through the layer. When the re-entry was first made, the wellhead pressure in Eugenie 1 was 30 psi (Van Sambeek, 2010); by the end of the day the wellhead pressure was 14 psi. The pressure in the cavity acting on the roof is the wellhead pressure plus the weight of the column of brine. The brine is assumed to have a density of 10 lbs/gal, which is referred to as ten pound brine (Van Sambeek, 2010). The present model makes the assumption that the entire cavern is under the same pressure. This simplification seems appropriate since the concern is for the short-term behavior of the overlying layers to the pressure acting on the cavern roof. The side and bottom effects caused by a pressure increase with depth due to the brine density are considered negligible. The pressure was then decreased at a steady rate from 30 to 14 psi at the wellhead for a simulated time period of 22 hrs, the duration of leak off. The change in leak off from 1 bbl/min to 3 bbl/min during the last hour was ignored. For the material models chosen for the overlying strata, a rate change in the pressure does not affect the behavior.

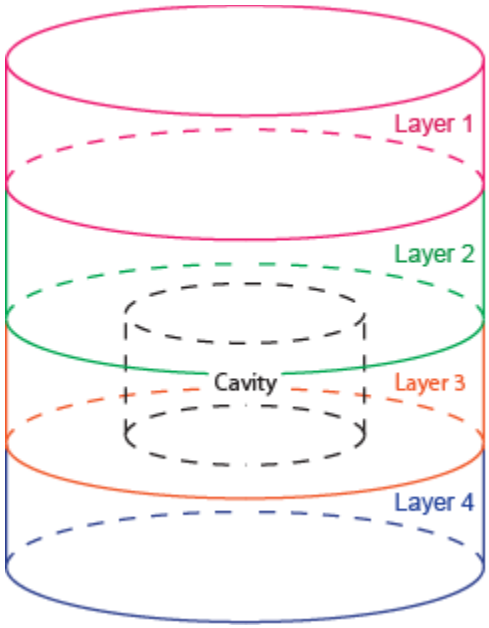

Figure 1. Model set-up schematic.

2 Site Stratigraphy and Finite Element Model

In any numerical simulation of physical processes it is frequently necessary to invoke a number of assumptions which render the analysis tractable. Analyses involving geologic materials are well known to be very challenging due to the extreme variability of rock quality and the inability to fully characterize the in-situ response of the rock when subjected to a disturbance. In addition, the formations being considered herein generally contain a number of layers of rock of various types and thicknesses. Typically these layers within the formations are not explicitly represented in the numerical model, but are assigned properties thought to be representative of the specific formation.

The stratigraphy for our FE model (shown in Figure 1) is based primarily on that provided by Goodman et al. (2009). It consists of four strata, namely (1) an alluvium, (2) the Rustler formation, (3) a salt layer, and (4) an underlying layer. Goodman et al. (2009) classify the salt as part of the Salado formation. According to Hendrickson and Jones (1952), the Salado formation, which lies between the Rustler and Castile formations in areas east of the Pecos River, is absent in most places west of the river. The Castile formation consists of redbeds, salt, gypsum, and anhydrite. The point is that the stratigraphy at this site is not well understood. The proposed drilling of additional boreholes with accurate borehole logging and collection of data pertaining to the rock physical properties will be quite valuable.

2.1 Alluvium

Henard et al. (2009) describe the alluvium as consisting of gravel, sand, and silt with beds of caliche and limestone/conglomerates. Hendrickson and Jones (1952) describe it as consisting of clay, silt, sand, gravel, caliche, and conglomerate, where the component materials are

irregularly distributed both horizontally and vertically. Bachman (1974) refers to the lime sand and lime pebble conglomerate cover as fanglomerates. The clasts in these deposits are derived almost entirely from Permian limestones and associated sedimentary rocks along the eastern side of the Guadalupe Mountains. In many places the limestone pebbles are cemented with calcium carbonate. According to Hendrickson and Jones (1952), the conglomerate may be so well cemented that it is reported to be limestone by well drillers. A dense caliche caprock usually less than 0.5 m (18 inch) thick is present at some places. The caprock is also structureless and appears to be cemented from locally derived solution of the limestone clasts.

Because of the variation of the alluvium, it is hard to characterize the material for modeling purposes with a single material description. Instead two materials – both modeled as homogeneous, isotropic, linear elastic – are suggested. The first material is a dense sand and gravel soil mixture. The US Army Corps of Engineers (USACE 1990) and Caltrans (2003) list representative elastic properties for this material, and Das (2006) and Holtz and Kovacs (1981) provide information about its density (Table 1). The values used in the finite element model, in general, represent the average values for the ranges given in Table 1 and are given in Table 2.

The second material is a weak limestone. Data for representative elastic properties was obtained from Palchik (2010). When considering the limestone data listed in Palchik, weak limestones were taken to have an unconfined compressive strength of less than 40 MPa (~6000 psi). The range of property values and their averages are listed in Table 3. The values used in the finite element model, in general, represent average values for the ranges given in Table 3 and are given in Table 4.

Table 1. Elastic properties for dense sand and gravel soils found in literature.

Soil Description	Range of Young's Moduli (MPa)	Range of Poison's Ratios	Range of Densities (kg/m^3)
Dense sand and gravel [1]	96 – 192	–	
Dense gravel [2]	96 – 192	0.3 – 0.4	
Dense angular-grained silty sand [3]			1940
Sands and gravel [4]			1500 – 2300

[1] USACE (1990) Table D-3, p. D-5
[2] Caltrans (2003) Table 4.4.7.2.2A, p. 4-19
[3] Das (2006) Table 3.2, p. 57
[4] Holtz and Kovacs (1981) Table 2-1, p. 15.

Table 2. Elastic properties for the alluvium when modeled in the present FE analysis as a dense sand and gravel soil.

Young's Modulus (MPa)	Poison's Ratio	Density (kg/m^3)
145	0.35	1920

Table 3. Elastic properties for five weak limestones, having an unconfined compressive strength less than 40 MPa, from Palchik (2010).

Soil Description	Range of Young's Moduli (MPa)	Range of Poison's Ratios	Range of Densities (kg/m^3)
Weak limestone	6200 – 35,400	0.15 – 0.32	1740 – 2360

Table 4. Elastic properties for the alluvium when modeled in the present FE analysis as a weak limestone.

Young's Modulus (MPa)	Poisson's Ratio	Density (kg/m^3)
15,000	0.25	2150

2.2 Rustler Formation

The Rustler formation is also treated as a homogeneous, isotropic, linear elastic material. Data for the mechanical properties of this layer were taken from Argüello et al. (2009), who were interested in this layer in the vicinity of the local potash mining areas. The mechanical properties used are listed in Table 5.

Table 5. Elastic properties for the Rustler formation used in the present FE calculations.

Young's Modulus (MPa)	Poisson's Ratio	Density (kg/m^3)
20,000	0.30	2160

2.3 Salt

The salt layer is modeled as a rate-dependent material using a multi-mechanism deformation (M-D) model proposed by Munson and Dawson (1979, 1982, 1984) and extended by Munson et al. (1989). The rock properties for the salt in the vicinity of I&W are not known, so for this analysis it is assumed to be similar to argillaceous WIPP salt. This material is well characterized and has been implemented into the M-D model on Sandia computers. A complete discussion of the M-D model is beyond the scope of this report; however, interested readers can access the Sandia reports above. The model parameters are listed in Table 6.

Table 6: Salt creep properties (Munson et al., 1989)

Parameters(Units)	Argillaceous Halite
A_1 (/sec)	1.407E23
Q_1 (cal/mole)	25,000
n_1	5.5
B_1 (/sec)	8.998E6
A_2 (/sec)	1.314E13
Q_2 (cal/mole)	10,000
n_2	5.0
B_2 (/sec)	4.289E-2
σ_0 (MPa)	20.57
Q	5,335
M	3.0
K_0	2.470E6
c (/T)	9.198E-3
α	-14.96
β	-7.738
δ	0.58

2.4 Cavern Shape and Its Modeling

One of the assumptions made in the following analyses is that the cavern is cylindrical in shape. As viewed from the top, the approximate shape of the Eugenie 1 cavern that was able to be surveyed by sonar was circular (see Figure 2). This portion of the cavern is commonly referred to as the upper cavern. In addition, dissolution of a salt cavern in a horizontally isotropic, homogeneous bedded salt formation should occur equally in all directions. After 40 years of operation, even a two well operation like that at I&W will eventually produce a circular-shaped dissolution cavern (personal communication with John Plosz and Peter Jackson, The Mosaic Company). Finally, a horizontally circular-shape is consistent with other solution mining activities such as brine caverns, liquid storage caverns, and mineral extraction. In the present analyses, the plan shape is more important than the geometry of the sides since the emphasis is on the deformation of overlying strata with changes in cavern pressure. The only information on the possible shape of the sides of the cavern come the SOCON sonar surveys of the upper Eugenie 1 cavern, which is shown in Figure 3. Due to the lack of information on the vertical shape, the caverns were modeled as cylindrical. A cylindrical geometry simplifies the finite element mesh and, as previously stated, the emphasis of the present analyses is on the response due to pressure on cavern roof.

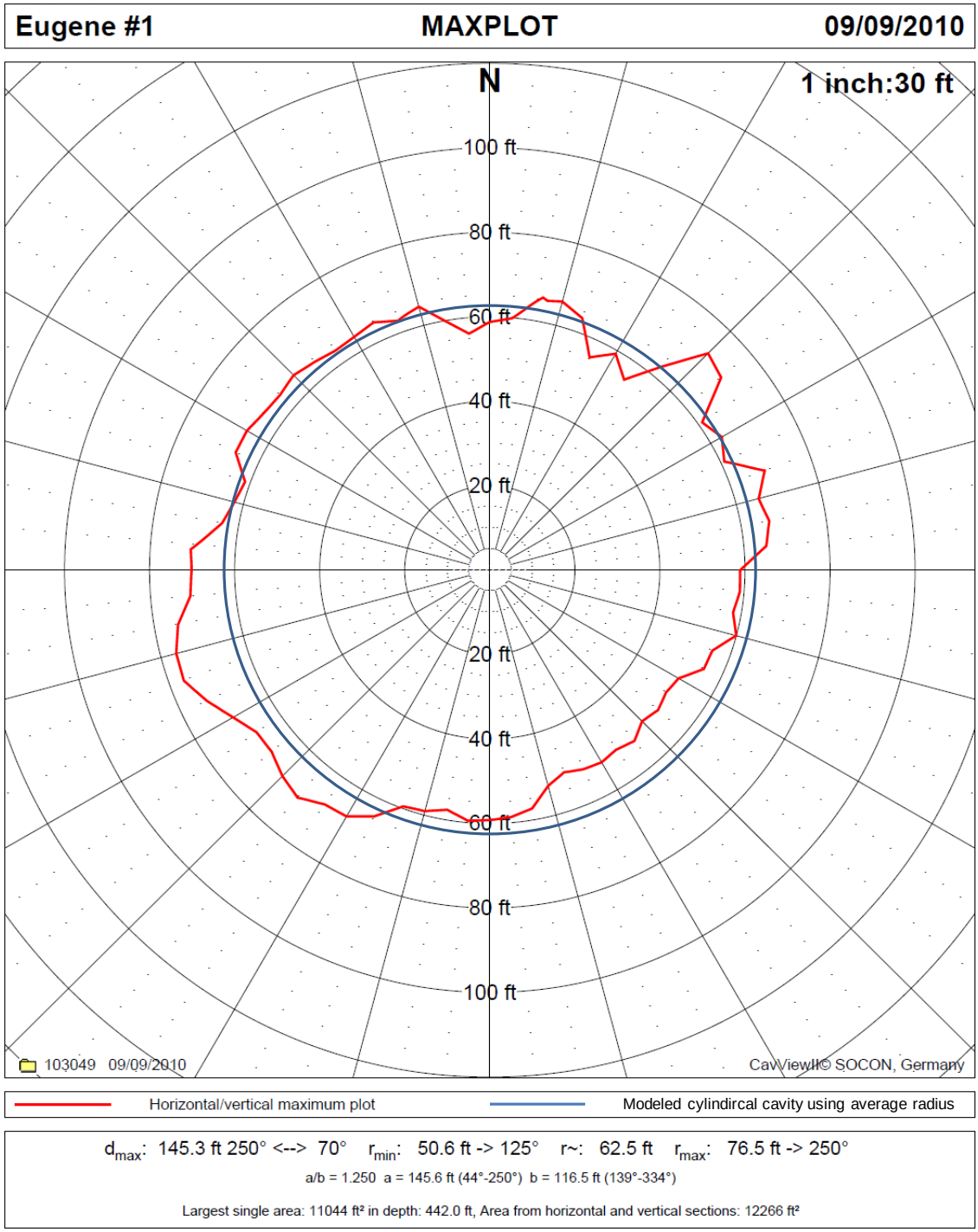

Figure 2. SOCON plot of horizontal/vertical maximum cavern extent, which occurs very close to the top of the upper Eugenie 1 cavern, in red (SOCON, 2010). Superimposed on the plot is a circular approximation of the cavern using the average cavern radius of 62.5 ft (19.1 m).

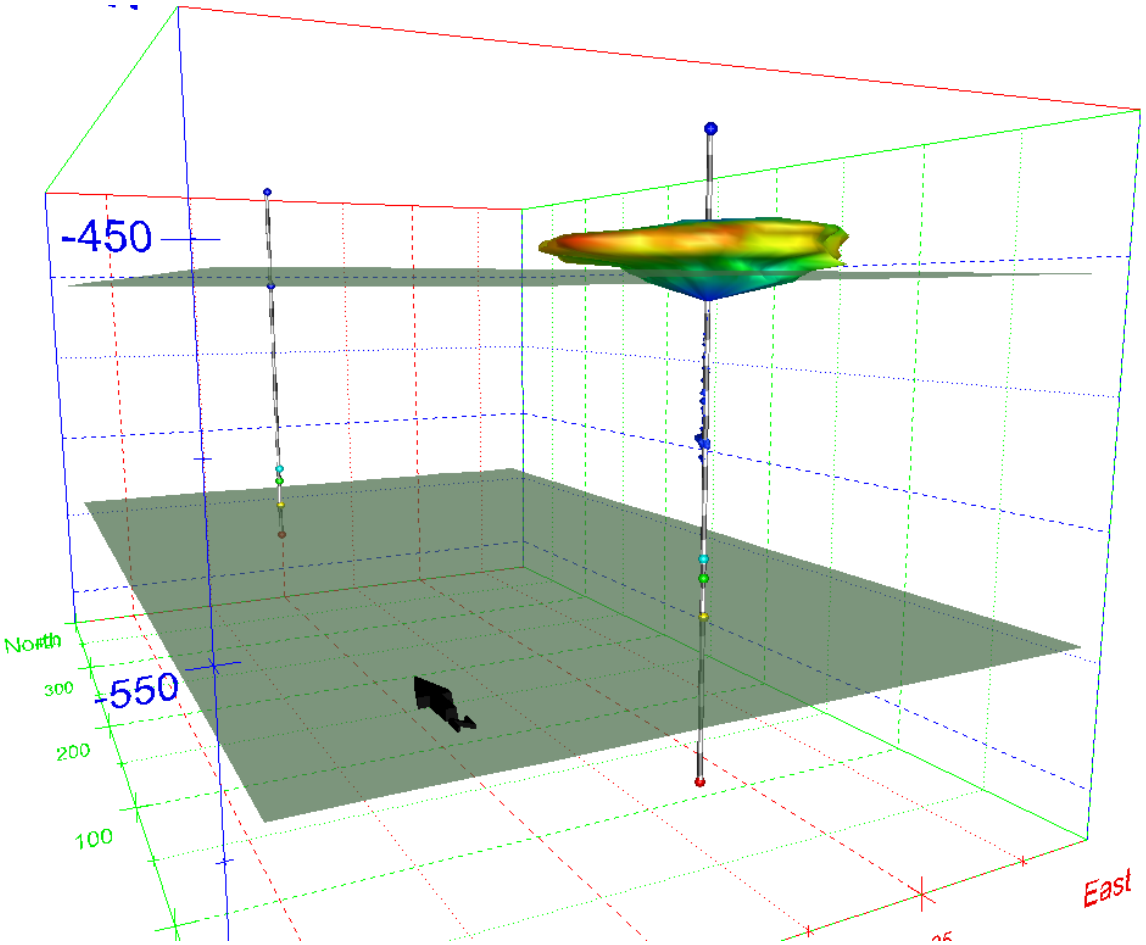

Figure 3. Plot of upper cavern along Eugenie 1.

In order to investigate the modeled tiltmeter response due to the change in pressure in the cavern during the re-entry, several cavern sizes were investigated. The first size (R1) is that of the average radius of the upper cavern along Eugenie 1, as shown in Figure 2. This size cavern was chosen to investigate whether the majority of the tiltmeter reading changes were due to pressure changes in the cavern. The second cavern size (R2) was chosen to match the horizontal size of the area showing seismic signature of cavern effects (Goodman et al., 2009) (Figure 4). The area was calculated to be 142,435 ft^2 (13,233 m^2). A circular area having that area would have a radius of 213 ft (64.9 m). The last modeled cavern size (R3) was based on the idea that maybe the cavern, containing the estimated missing volume of 0.9 – 1.2 million barrels, was somehow confined to below the blue shale stringer in the 16 ft thick salt layer. The cylindrical radius of this cavern would be approximately 350 ft (106 m). Figure 5 shows a plot of this size cavern overlain on earlier interpretations of the seismic data. The earlier seismic interpretaions were from a NMOCD public presentation on Oct 28, 2009. They were used because their areal extent is slightly larger than the final interpretation by Goodman et al. (2009). The largest cavern, if centered at Eugenie 1, would extend beyond Eugenie 2. The cavern sizes are summarized in Table 7.

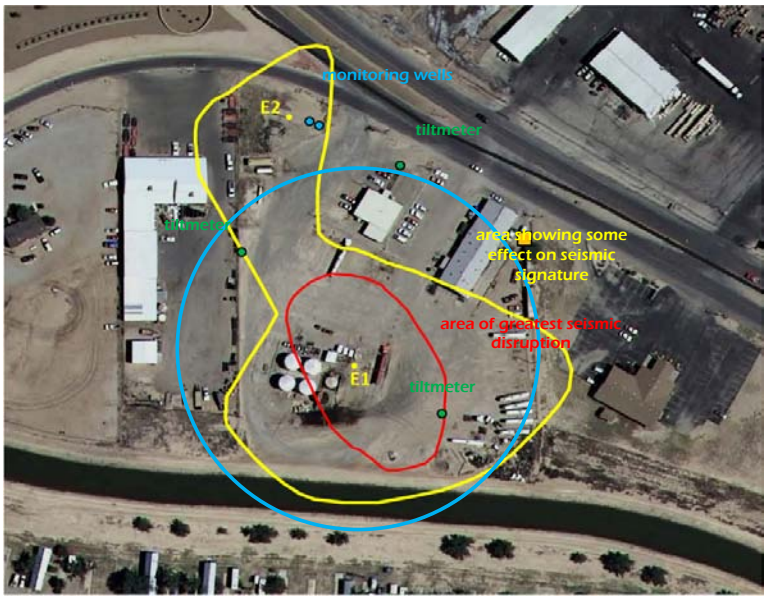

Figure 4. Final interpretation of seismic data (Goodman et al, 2009) with a circle with radius = 213 ft , 64.9 m superimposed.

Figure 5. Early interpretations of seismic data from a NMEMNRD public presentation dated Oct 28, 2009 with a circle with radius = 350 ft superimposed. The cavern, if centered at Eugenie 1, extends beyond Eugenie 2.

Table 7. Summary of cylindrical cavern sizes and their designation used in the current analyses.

Designation	Radius (ft)	Radius (m)
R1	62.5	19.1
R2	213	64.9
R3	350	106.7

Besides the uncertainty of the size of the brine cavern at the I&W facility, its location is also unknown. The majority of the estimated dissolved salt volume was not located during the two re-entry attempts. The seismic signature interpretations suggest that the majority of the cavern should be centered around Eugenie 1. However, the seismic signature interpretations also show the cavern could be partly under Eugenie 2. In an attempt to account for the uncertainty in the cavern location, two centers for the cylindrical models were chosen. The first center is along Eugenie 1. The second center is at the midpoint between Eugenie 1 and Eugenie 2.

The meshes used for the modeling are shown in Figures 6 through 8. In all cases the boundary conditions are such that there are no displacement boundaries on the *x*-face (east and west direction), *y*-face (north and south direction), and *z*-face (bottom). Gravity is invoked so that the vertical stress increases according to the density of the layers. Pressure equal to the weight of the brine at the depth of the top of the salt plus the wellhead pressure was applied to the interior of the cavern. The pressure was decayed linearly from the initial wellhead pressure of 30 psi to the final wellhead pressure of 14 psi over a 22 hour period to simulate the actual field conditions during the leak off.

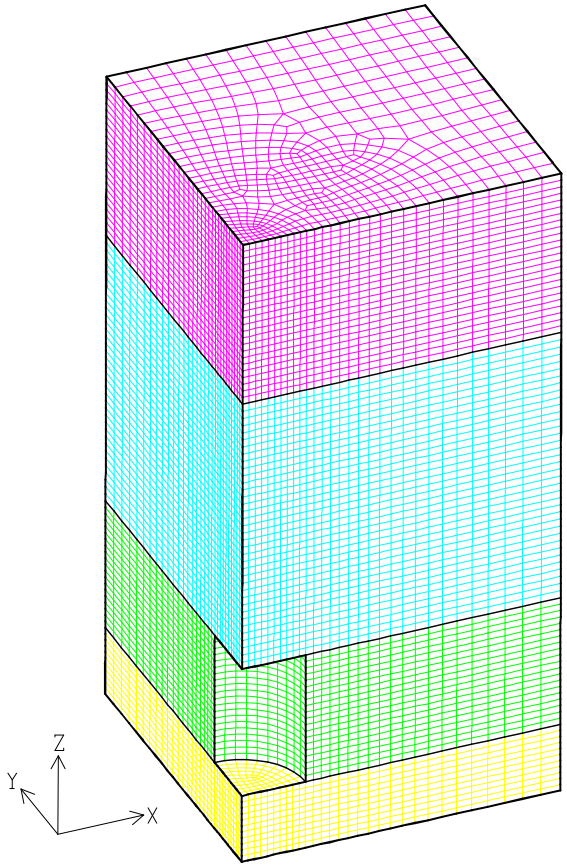

Figure 6.Mesh used in analyses involving caverns having a size R1 = 19.1 m. X is east, Y is north, and Z is up. The surface is at Z = 0.

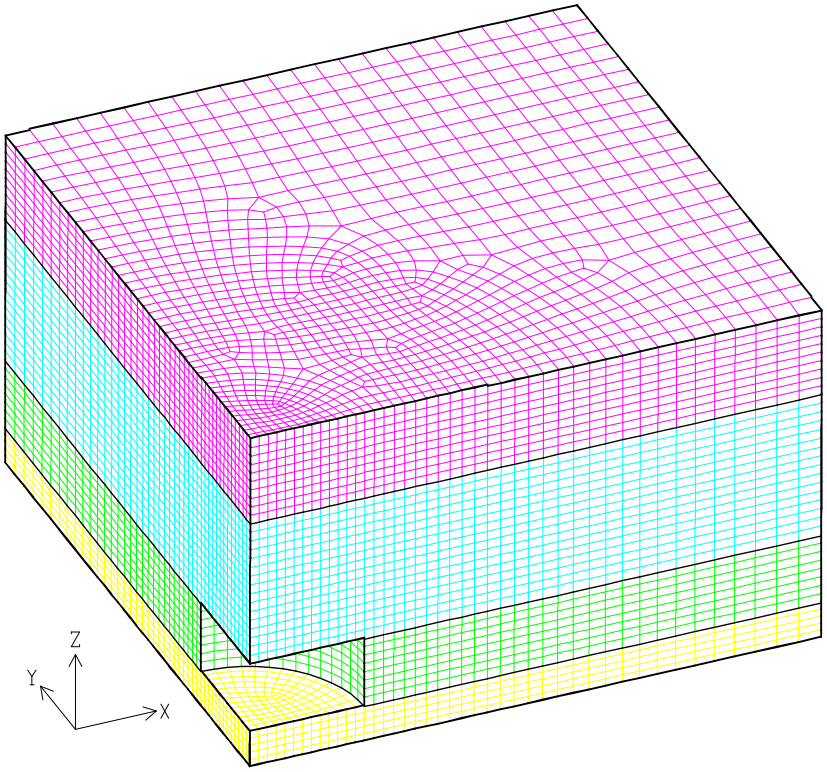

Figure 7. Mesh used for analyses involving cavern sizes of R2 = 64.9 m. X is east, Y is north, and Z is up. The surface is at Z = 0.

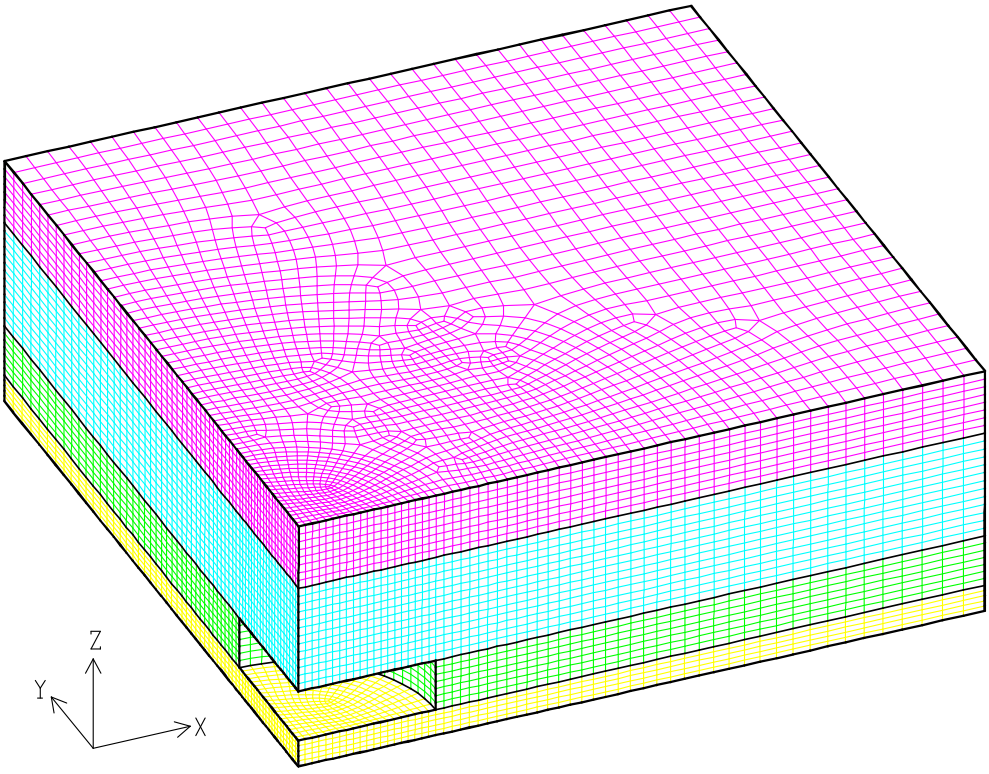

Figure 8. Mesh used for analyses involving cavern sizes of R3 = 106.7 m. X is east, Y is north, and Z is up. The surface is at Z = 0.

2.5 Computer Codes

The finite element code used in the present calculations is JAS3D, version 2.4.C (Blanford, 2001). It uses an eight-node hexahedral Lagrangian uniform strain element with hourglass stiffness to control zero energy modes. A nonlinear conjugate gradient method is used to solve the nonlinear system of equations. This efficient solution scheme is considerably faster than the direct solvers which are used in most commercial codes and is a product of decades of research and development into nonlinear, large strain finite element analyses. JAS3D includes at least 30 different material models. Two material models were chosen for use in the model described in this report: an elastic model for two overlying layers and the bottom layer and the M-D creep model for the salt. Related codes used in conjunction with JAS3D are CUBIT – a mesh generating program, APREPRO – a preprocessing program, and BLOT – a postprocessing program. All these codes are Sandia National Laboratories' products. Data processing was performed using Microsoft Excel.

3 Analysis Results

3.1 Methodology

To determine the calculated surface tilts we first located the node on the model meshes that was closest to the position where the tiltmeters would be. For the tiltmeters that lie outside of the quadrant that was meshed, symmetry was used to reflect their position to within the grid. Due to the expected symmetric deformation of the model, the distance was thought to be more important than location. In general, we were able to find nodes that are within a meter of the tiltmeter distances, even though the nodal positions were off by several meters. If the distances were off by more than a couple meters, another node was used so that the average of the two nodal distances was approximately the same as the distance to the tiltmeter being considered. Comparisons of the tiltmeter and nodal coordinates and distances from the center of the grid are given in Tables 8 and 9. For the data in Table 8, the center is assumed to be Eugenie 1; for Table 9, the center is assumed to be the midpoint between Eugenie 1 and Eugenie 2. Since the upper cavity is physically at Eugenie 1, the smaller cavern radius R1 was not used in analyses where the cavern is assumed centered at the midpoint between the two wells, Eugenie 1 and 2.

Table 8. Comparison of tiltmeter versus nodal coordinates and distances from the center of the mesh, considered here to be Eugenie 1. For the analyses, having better distance estimates was considered more important than matching the coordinates due to the expected symmetrical deformation of the model.

Mesh and Entity	X-coordinate (m)	Y-coordinate (m)	Distance from Eugenie 1 (m)
R1 mesh			
Tiltmeter 8536	38.3	38.9	54.6
Node 11894	36.9	40.5	54.8
Tiltmeter 8292	19.5	79.3	81.7
Node 11711	22.5	78.6	81.8
Tiltmeter 8260	36.7	12.2	38.6
Node 11653	37.6	9.8	38.8
R2 mesh			
Tiltmeter 8536	38.3	38.9	54.6
Node 12635	38.0	37.9	53.7
Tiltmeter 8292	19.5	79.3	81.7
Node 10188	6.8	81.8	82.1
Tiltmeter 8260	36.7	12.2	38.6
Node 12669	37.2	9.3	38.3
R3 mesh			
Tiltmeter 8536	38.3	38.9	54.6
Node 18450	38.4	38.4	54.3
Tiltmeter 8292	19.5	79.3	81.7
Node 18175	12.3	77.7	78.7
Node 18186	19.7	81.5	83.7
Tiltmeter 8260	36.7	12.2	38.6
Node 18402	33.4	17.7	37.8

Table 9. Comparison of tiltmeter versus nodal coordinates and distances from the center of the mesh, considered here to be the midpoint between Eugenie 1 and Eugenie 2. For the analyses, having better distance estimates was considered more important than matching the coordinates due to the expected symmetrical deformation of the model.

Mesh and Entity	X-coordinate (m)	Y-coordinate (m)	Distance from Eugenie 1 (m)
R2 mesh			
Tiltmeter 8536	24.8	8.2	26.1
Node 12701	22.0	12.5	25.4
Tiltmeter 8292	33.0	32.2	46.1
Node 12633	31.3	31.2	44.2
Node 12634	34.5	34.4	48.7
Tiltmeter 8260	50.2	59.3	77.6
Node 10475	46.0	65.2	79.7
R3 mesh			
Tiltmeter 8536	24.8	8.2	26.1
Node 18369	25.9	4.6	26.4
Tiltmeter 8292	33.0	32.2	46.1
Node 18431	35.3	30.6	46.8
Tiltmeter 8260	50.2	59.3	77.6
Node 18234	43.6	59.2	73.5
Node 18245	51.4	59.1	79.0

To calculate the tilts, the nodes on the next layer down matching the *x*- and *y*-coordinates of the surface nodes in Tables 8 and 9 were used. For the R1 mesh, this layer is 4.3 m below the surface; for the R2 mesh, it is 5.2 m below; and for the R3 mesh, it is 6.5 m below. A vector $\boldsymbol{R}$ which points from the node point below the surface to the corresponding node point on the surface was constructed. If the node point on the lower surface is *A* with coordinates (x_A, y_A, z_A) and the node point on the surface is *B* with coordinates (x_B, y_B, z_B), then the vector connecting *A* to *B* is given by:

$$\boldsymbol{R} = (x_B - x_A)\hat{\boldsymbol{i}} + (y_B - y_A)\hat{\boldsymbol{j}} + (z_B - z_A)\hat{\boldsymbol{k}}$$

In component form this is written as:

$$\boldsymbol{R} = R_x\hat{\boldsymbol{i}} + R_y\hat{\boldsymbol{j}} + R_z\hat{\boldsymbol{k}}$$

The length of the vector is:

$$|\boldsymbol{R}| = \sqrt{R_x^2 + R_y^2 + R_z^2}$$

The direction cosines of ***R*** (Figure 9) are defined as:

$$l = \cos\alpha = \frac{R_x}{|\boldsymbol{R}|}$$

$$m = \cos\beta = \frac{R_y}{|\boldsymbol{R}|}$$

$$n = \cos\gamma = \frac{R_z}{|\boldsymbol{R}|}$$

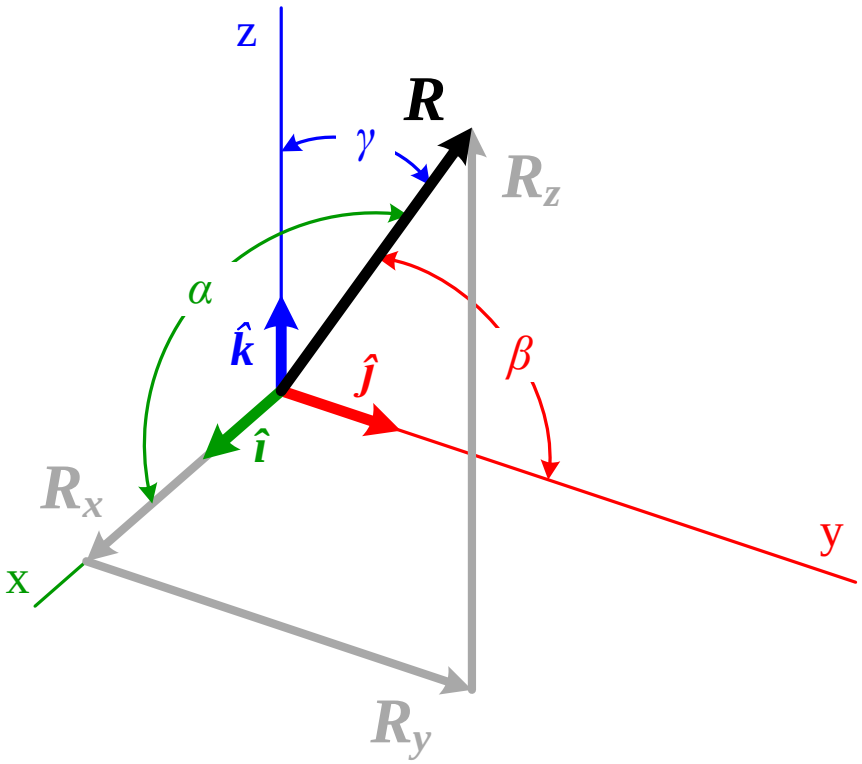

Figure 9. Diagram showing various vector definitions.

Since γ is the angle between the z-axis and the vector, it is the angle of tilt. If needed at some future time, components R_x and R_y could be used to determine the direction the vector tilts in the *xy*-plane. Due to symmetry, the model cavern should tilt toward the central point in the mesh.

3.2 Comparison of Field Measurements with Predicted Values

Plots of the predicted change in tilts versus the actual measured change in tilts are shown in the following figures. In these figures the absolute values of the tilts are plotted against time. Time was used because the field pressure data is somewhat spotty. Time and cavern pressure are linearly related in the FE analyses. The plots are only concerned with the change in tilt over the

22 hour time frame that the cavern brine was bled off. The present model cannot capture the deformation history that the I&W site has undergone. However, by zeroing the initial tilt for both the actual field data and the FE analyses, a comparison the behaviors is possible.

The first six plots (Figures 10 – 15) are of the absolute value of the change in tilt for three tiltmeters when the cavern center is at Eugenie 1 compared to the measured field data. As stated previously, the alluvium was modeled as both a sand and gravel soil and as a weak limestone. Information on the rock mechanics properties of the Rustler formation came from past Sandia National Laboratories studies. The second six plots (Figures 16 – 21) are of the absolute value of the change in tilt for three tiltmeters when the cavern center is at the midpoint between Eugenie 1 and Eugenie 2 compared to the measured field data. Since the upper cavern is physically centered at Eugenie 1, R1 was not used in analyses where the cavern is centered at the midpoint between Eugenie 1 and 2.

As expected, the larger the cavern, the greater its tilt. Also, tilts for the models where the alluvium is assumed to behave as a sand and gravel soil are greater than those models where the alluvium is assumed to behave as a weak limestone. This is because the modulus of elasticity of the limestone is about 100 times greater than that of the soil, making for a much stiffer layer. Also, as the pressure is reduced in the caverns, i.e. as time increases, the tilt increases. These facts give assurance that the finite element model is accurately predicting the physical conditions.

Any tilt resulting from the upper Eugenie 1 cavern is negligible (Figures 10 – 15). At every tiltmeter location, the tilt caused by the upper cavern is but a fraction of a microradian.

Even the largest changes in tilts for the biggest cavern modeled, no matter where it was centered, were generally less than the actual field measurements. In many cases, the predicted tilts are less than half the measured values. The implication is that the actual cavern diameter is much larger than what was modeled. Further modeling with larger cavern radii is necessary if this method to constrain the cavern size is to be continued in future analyses.

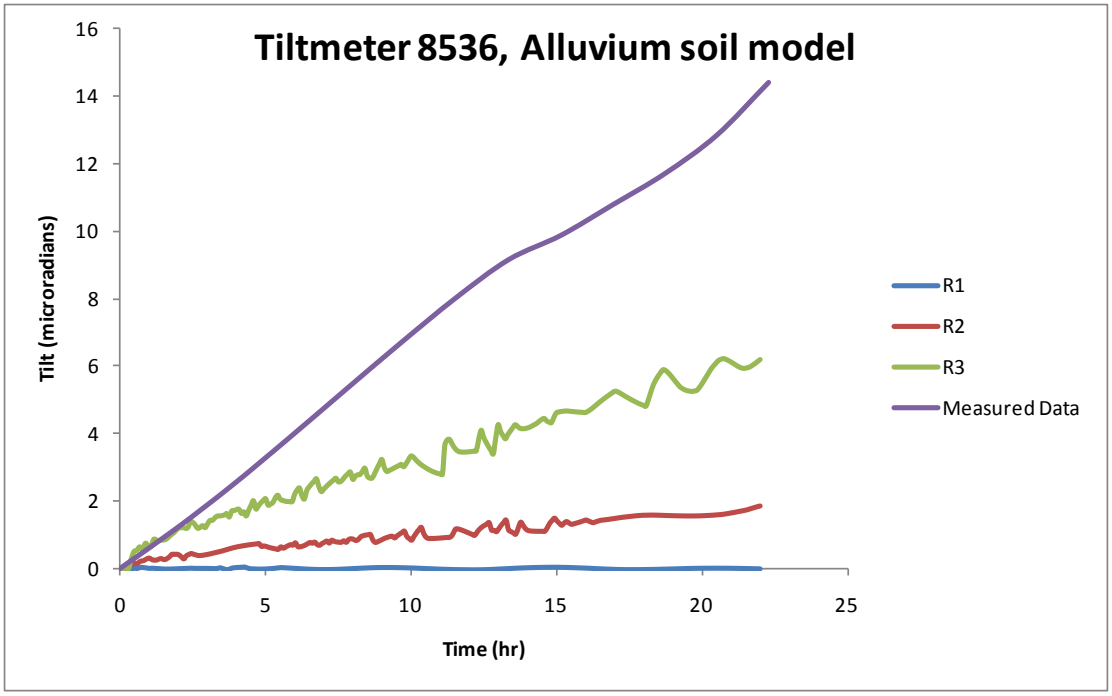

Figure 10. Absolute value of the change in tilt at Tiltmeter 8536 for the three different modeled cavern radii centered at Eugenie 1 compared to the field data. During the 22 hr cavern bleed off period the surface wellhead pressure dropped from 30 to 14 psi. The alluvium was modeled as a sand and gravel soil. R1 = 62.5 ft = 19.1 m, R2 = 213 ft = 64.9 m, and R3 = 350 ft = 106.7 m.

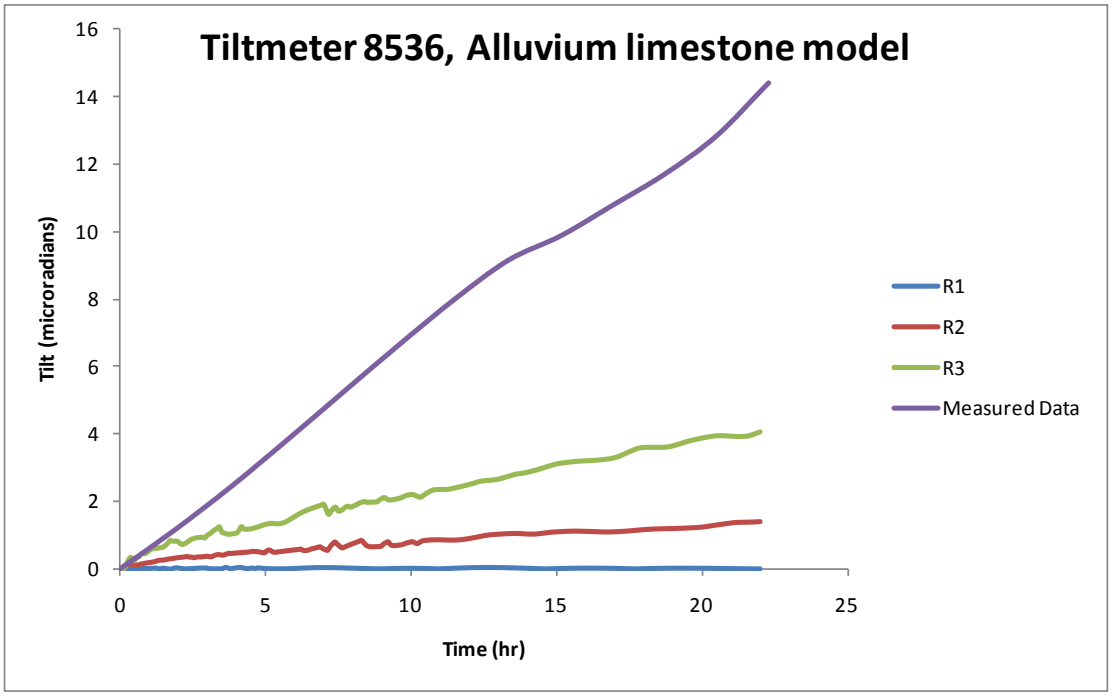

Figure 11. Absolute value of the change in tilt at Tiltmeter 8536 for the three different modeled cavern radii centered at Eugenie 1 compared to the field data. During the 22 hr cavern bleed off period the surface wellhead pressure dropped from 30 to 14 psi. The alluvium was modeled as a weak limestone. R1 = 62.5 ft = 19.1 m, R2 = 213 ft = 64.9 m, and R3 = 350 ft = 106.7 m.

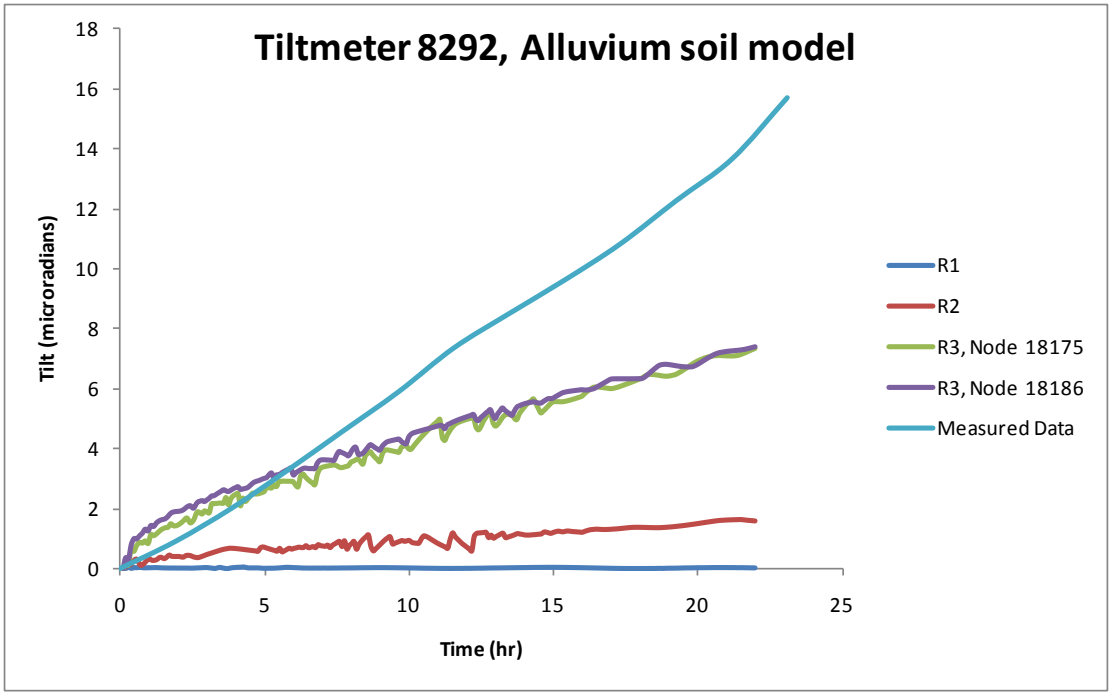

Figure 12. Absolute value of the change in tilt at Tiltmeter 8292 for the three different modeled cavern radii centered at Eugenie 1 compared to the field data. During the 22 hr cavern bleed off period the surface wellhead pressure dropped from 30 to 14 psi. The alluvium was modeled as a sand and gravel soil. R1 = 62.5 ft = 19.1 m, R2 = 213 ft = 64.9 m, and R3 = 350 ft = 106.7 m.

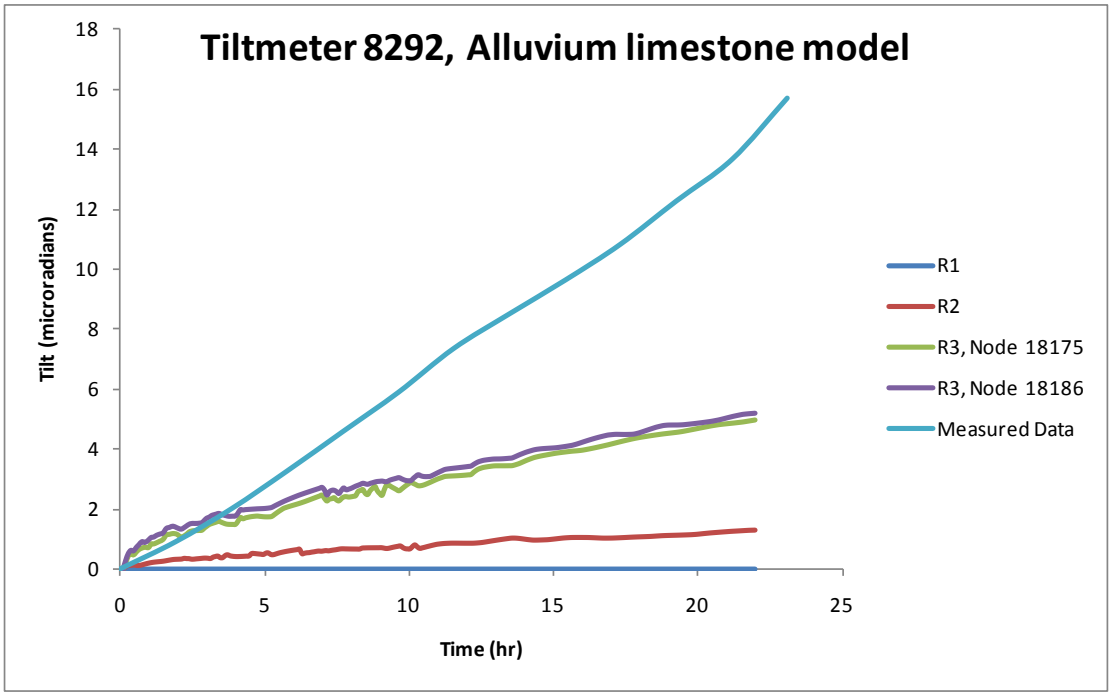

Figure 13. Absolute value of the change in tilt at Tiltmeter 8292 for the three different modeled cavern radii centered at Eugenie 1 compared to the field data. During the 22 hr cavern bleed off period the surface wellhead pressure dropped from 30 to 14 psi. The alluvium was modeled as a weak limestone. R1 = 62.5 ft = 19.1 m, R2 = 213 ft = 64.9 m, and R3 = 350 ft = 106.7 m.

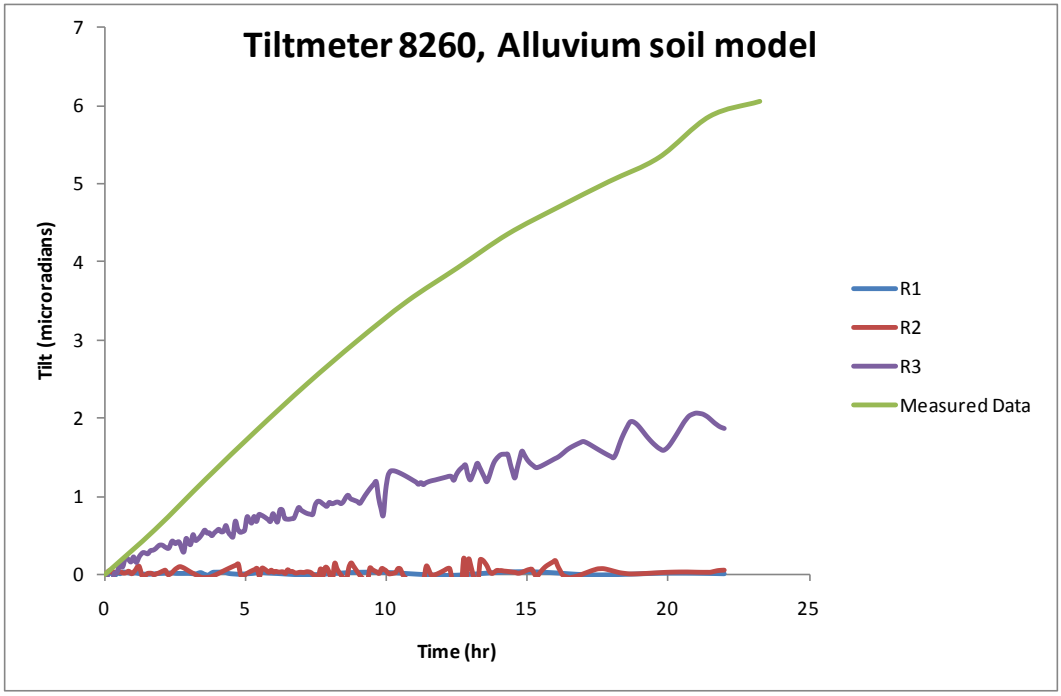

Figure 14. Absolute value of the change in tilt at Tiltmeter 8260 for the three different modeled cavern radii centered at Eugenie 1 compared to the field data. During the 22 hr cavern bleed off period the surface wellhead pressure dropped from 30 to 14 psi. The alluvium was modeled as a sand and gravel soil. R1 = 62.5 ft = 19.1 m, R2 = 213 ft = 64.9 m, and R3 = 350 ft = 106.7 m.

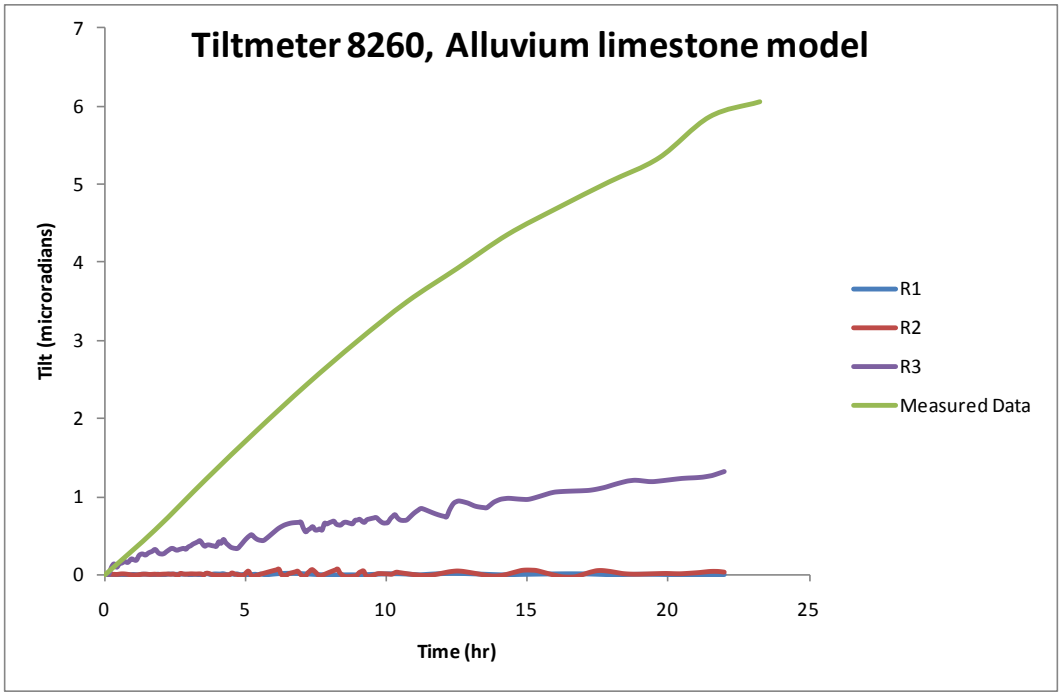

Figure 15. Absolute value of the change in tilt at Tiltmeter 8260 for the three different modeled cavern radii centered at Eugenie 1 compared to the field data. During the 22 hr cavern bleed off period the surface wellhead pressure dropped from 30 to 14 psi. The alluvium was modeled as a weak limestone. R1 = 62.5 ft = 19.1 m, R2 = 213 ft = 64.9 m, and R3 = 350 ft = 106.7 m.

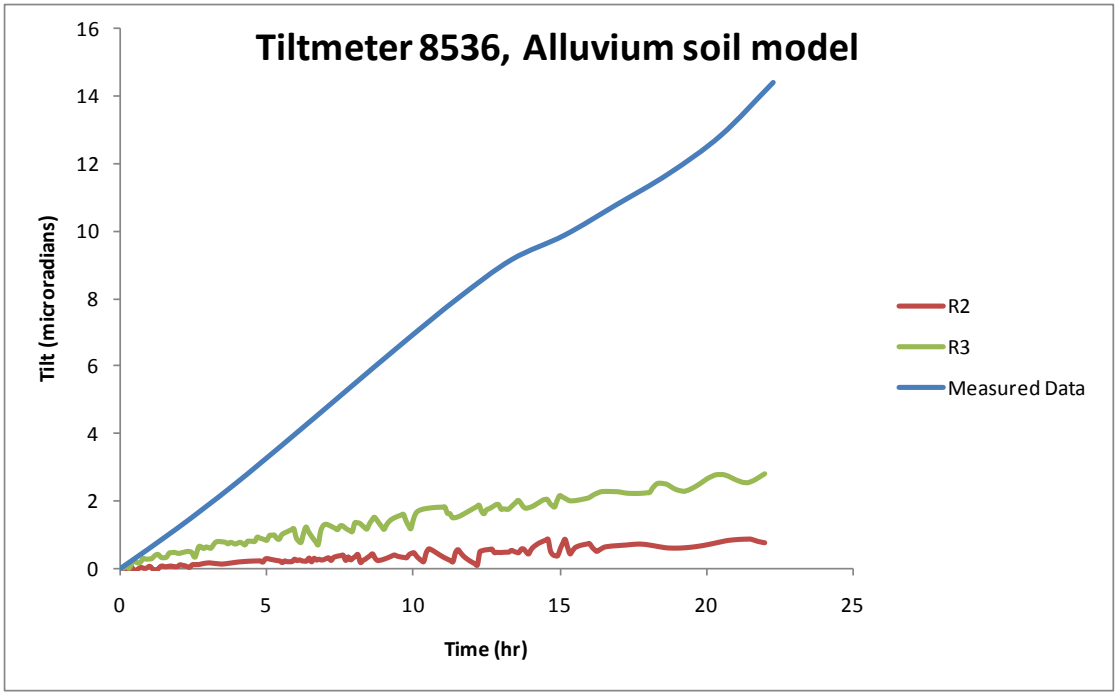

Figure 16. Absolute value of the change in tilt at Tiltmeter 8536 for the two different modeled cavern radii centered at the midpoint between Eugenie 1 and 2 compared to the field data. During the 22 hr cavern bleed off period the surface wellhead pressure dropped from 30 to 14 psi. The alluvium was modeled as a sand and gravel soil. R2 = 213 ft = 64.9 m and R3 = 350 ft = 106.7 m.

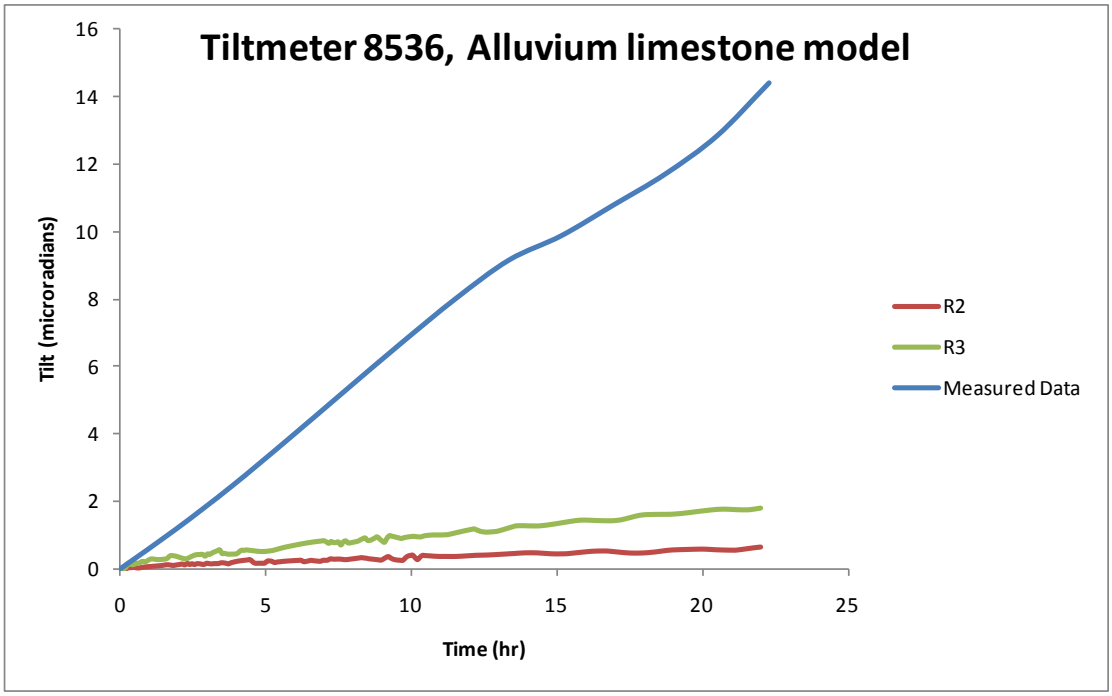

Figure 17. Absolute value of the change in tilt at Tiltmeter 8536 for the two different modeled cavern radii centered at the midpoint between Eugenie 1 and 2 compared to the field data. During the 22 hr cavern bleed off period the surface wellhead pressure dropped from 30 to 14 psi. The alluvium was modeled as a weak limestone. R2 = 213 ft = 64.9 m and R3 = 350 ft = 106.7 m.

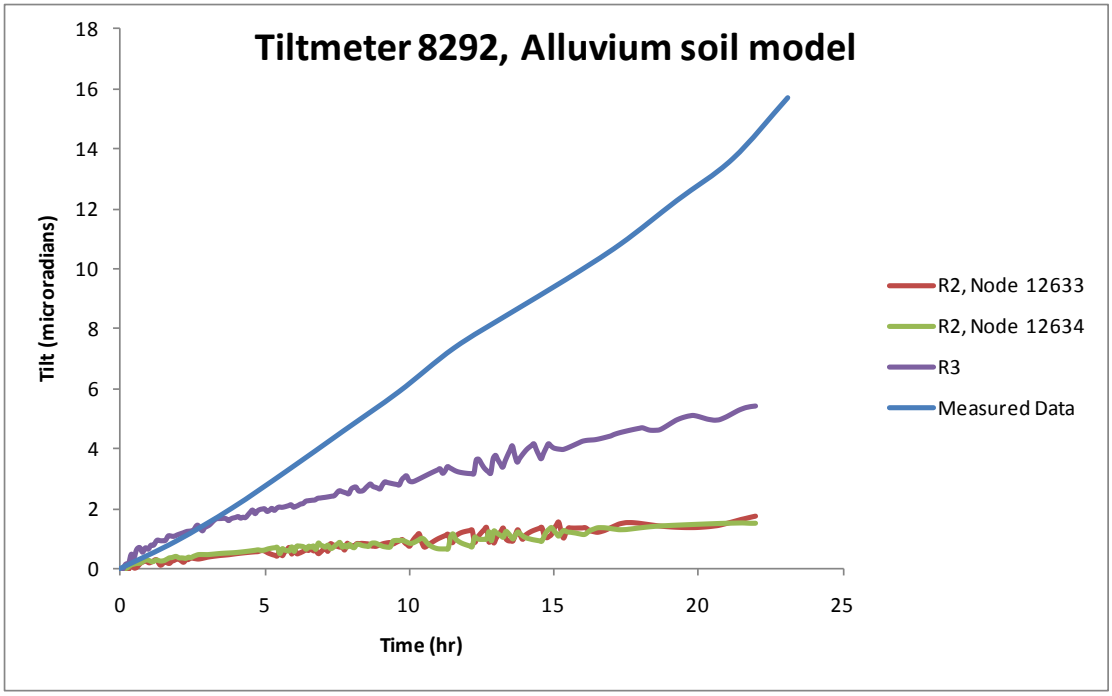

Figure 18. Absolute value of the change in tilt at Tiltmeter 8292 for the two different modeled cavern radii centered at the midpoint between Eugenie 1 and 2 compared to the field data. During the 22 hr cavern bleed off period the surface wellhead pressure dropped from 30 to 14 psi. The alluvium was modeled as a sand and gravel soil. R2 = 213 ft = 64.9 m and R3 = 350 ft = 106.7 m.

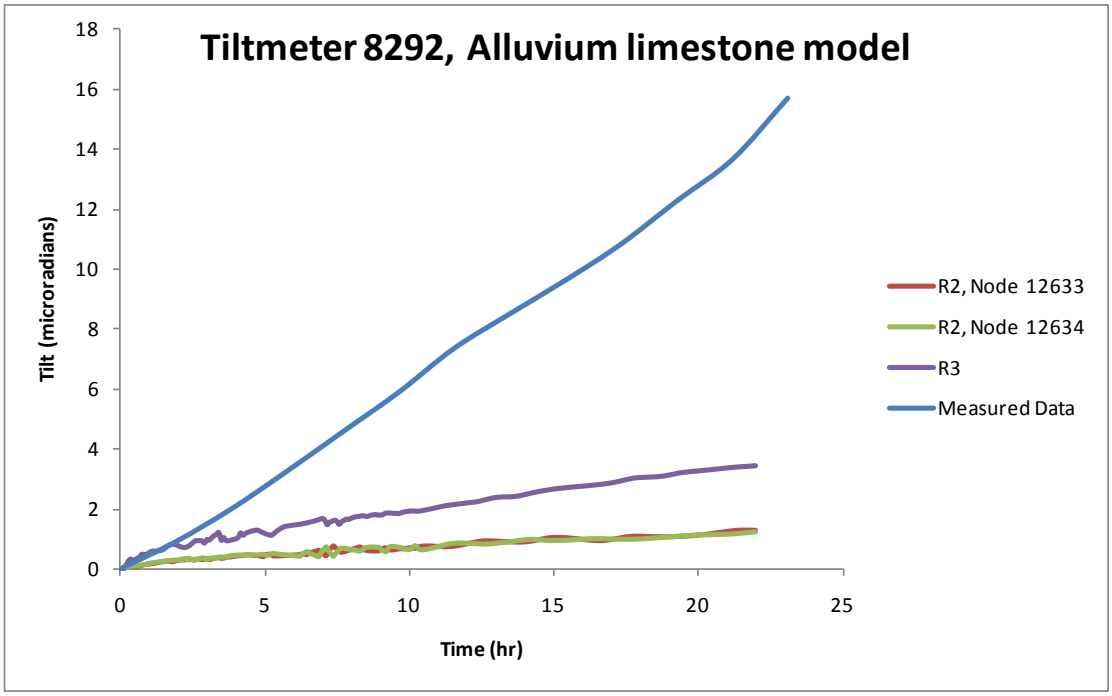

Figure 19. Absolute value of the change in tilt at Tiltmeter 8292 for the two different modeled cavern radii centered at the midpoint between Eugenie 1 and 2 compared to the field data. During the 22 hr cavern bleed off period the surface wellhead pressure dropped from 30 to 14 psi. The alluvium was modeled as a weak limestone. R2 = 213 ft = 64.9 m and R3 = 350 ft = 106.7 m.

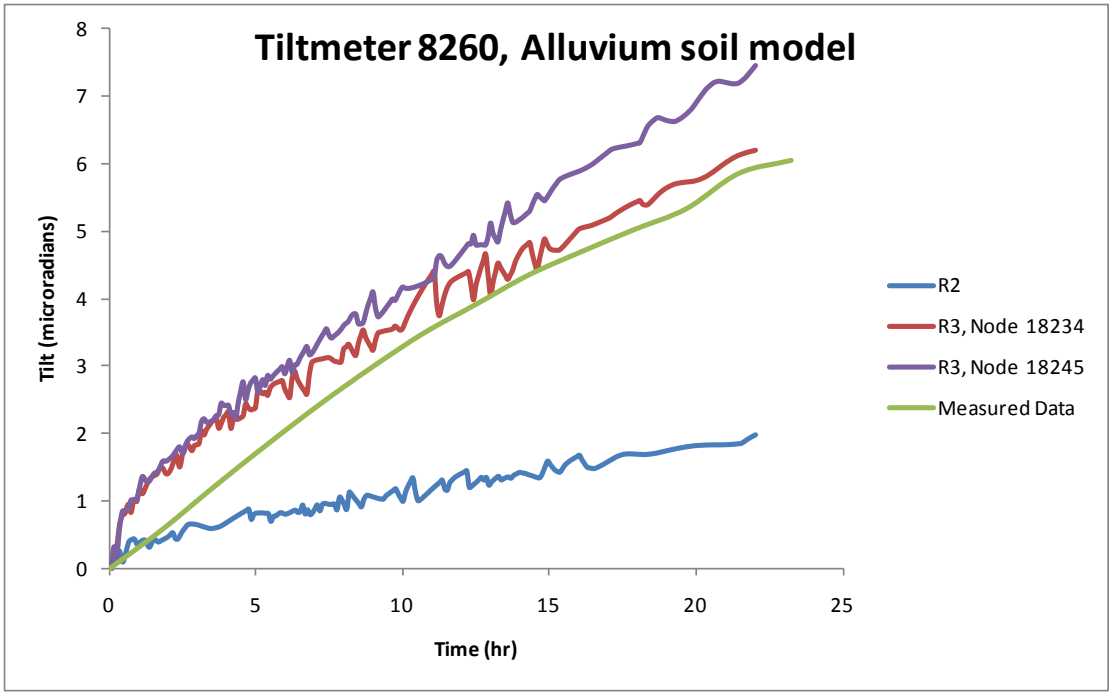

Figure 20. Absolute value of the change in tilt at Tiltmeter 8260 for the two different modeled cavern radii centered at the midpoint between Eugenie 1 and 2 compared to the field data. During the 22 hr cavern bleed off period the surface wellhead pressure dropped from 30 to 14 psi. The alluvium was modeled as a sand and gravel soil. R2 = 213 ft = 64.9 m and R3 = 350 ft = 106.7 m.

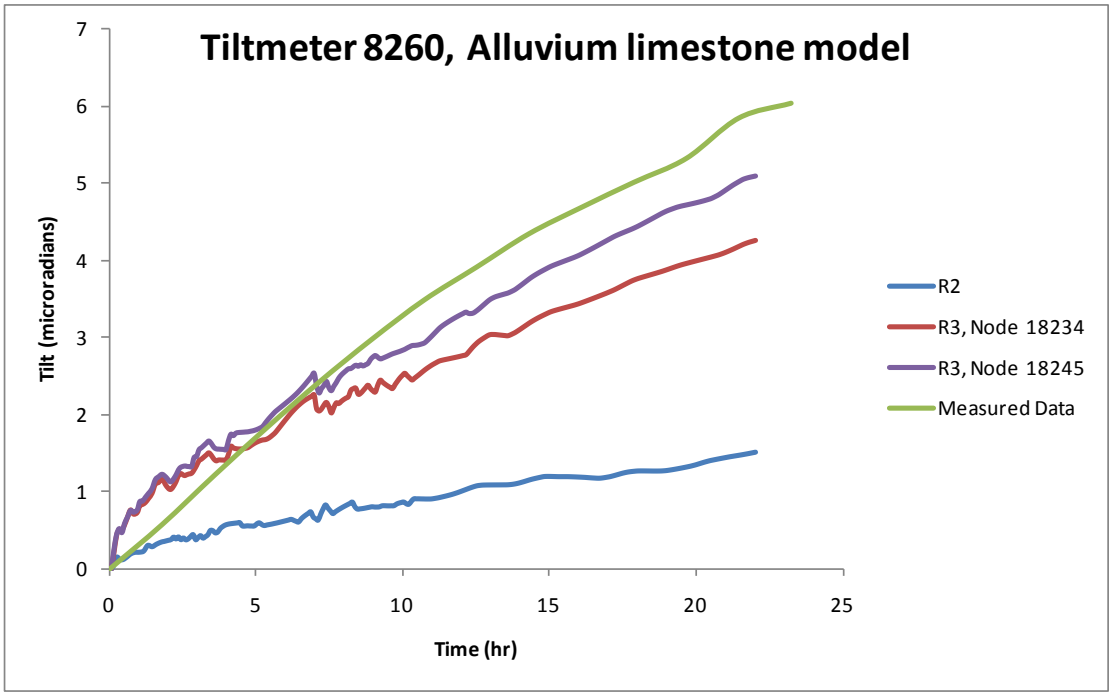

Figure 21. Absolute value of the change in tilt at Tiltmeter 8260 for the two different modeled cavern radii centered at the midpoint between Eugenie 1 and 2 compared to the field data. During the 22 hr cavern bleed off period the surface wellhead pressure dropped from 30 to 14 psi. The alluvium was modeled as a weak limestone. R2 = 213 ft = 64.9 m and R3 = 350 ft = 106.7 m.

3.3 Extrapolation of Numerical Results

It is of interest to attempt to extrapolate the present analyses results to match the measured field tilt changes. According to John Plosz and Peter Jackson of The Mosaic Company, for mature two well solution mining operations, which would include the I&W facility, the cavern tends to become circular in horizontal shape and centered at the midpoint between the two wells. Therefore, the data used for the extrapolation attempt will emphasize the two cavern radii used in the analyses where the cavern center was at the midpoint of Eugenie 1 and 2.

In the following figures we plot the maximum tilt changes seen in the analyses of the two cavern sizes over the time period of interest. The trend of the calculated results for each of the three tiltmeters is extrapolated until the measured change in tilt in field data is reached. The use of two data points to establish a trend is always rather uncertain, so two fits were used in the extrapolation. The first is a linear fit through the numerical results; the second is a logarithmic fit.

The Figures 22 and 23 show the results of the linear extrapolation. Figure 22 is for the case where the alluvium is modeled as a sand and gravel soil; Figure 23 is for the case where the alluvium is modeled as a weak limestone. For a specific tiltmeter, the line through the numerically predicted data is extended until the maximum observed change in tilt for that tiltmeter is reached. This produces estimates of a circular cavern radius necessary to produce the observed tilt changes. The tables inset in the plots indicate the results. The observed tilt changes for Tiltmeter 8536 require the largest cavern radii: 1200 ft for the soil alluvium model and 1900 ft for the weak limestone alluvium model. The difference is attributed to the higher stiffness that the limestone model has which requires a larger cavern radius to obtain the same change in tilt. The field data for Tiltmeter 8292 required the next largest cavern diameters. For the soil model, a cavern radius of 720 ft would be required; and for the limestone model, a cavern radius of about 1130 ft (using the average of the nodal predictions) is needed to obtain the observed deformation. The data for Tiltmeter 8260 matched the observed data fairly well for the R3-size cavern (Figures 20 and 21), so the extrapolated results do not suggest a much larger cavern.

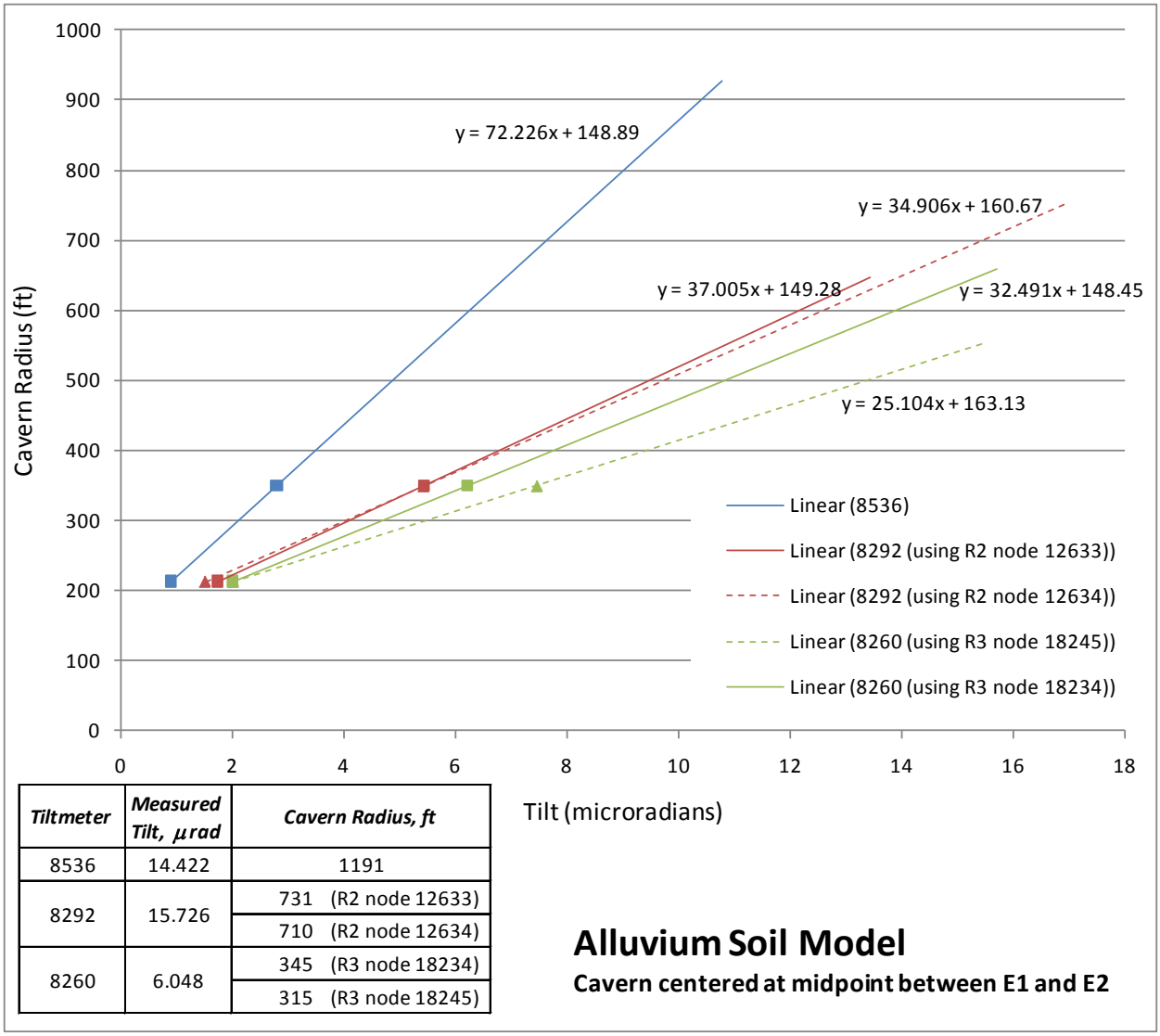

Tiltmeter	*Measured Tilt, μrad*	*Cavern Radius, ft*
8536	14.422	1191
8292	15.726	731 (R2 node 12633)
		710 (R2 node 12634)
8260	6.048	345 (R3 node 18234)
		315 (R3 node 18245)

Figure 22. Linear extrapolation of the predicted maximum changes in tilt over the 22 hr period of cavern bleed off for R2 and R3 cavern sizes in models where the alluvium is modeled as a sand and gravel soil. The cavern is assumed to be centered at the midpoint between Eugenie 1 and 2. The inset table lists the circular cavern radius that would be required to produce the observed tilt changes at the specific tiltmeter.

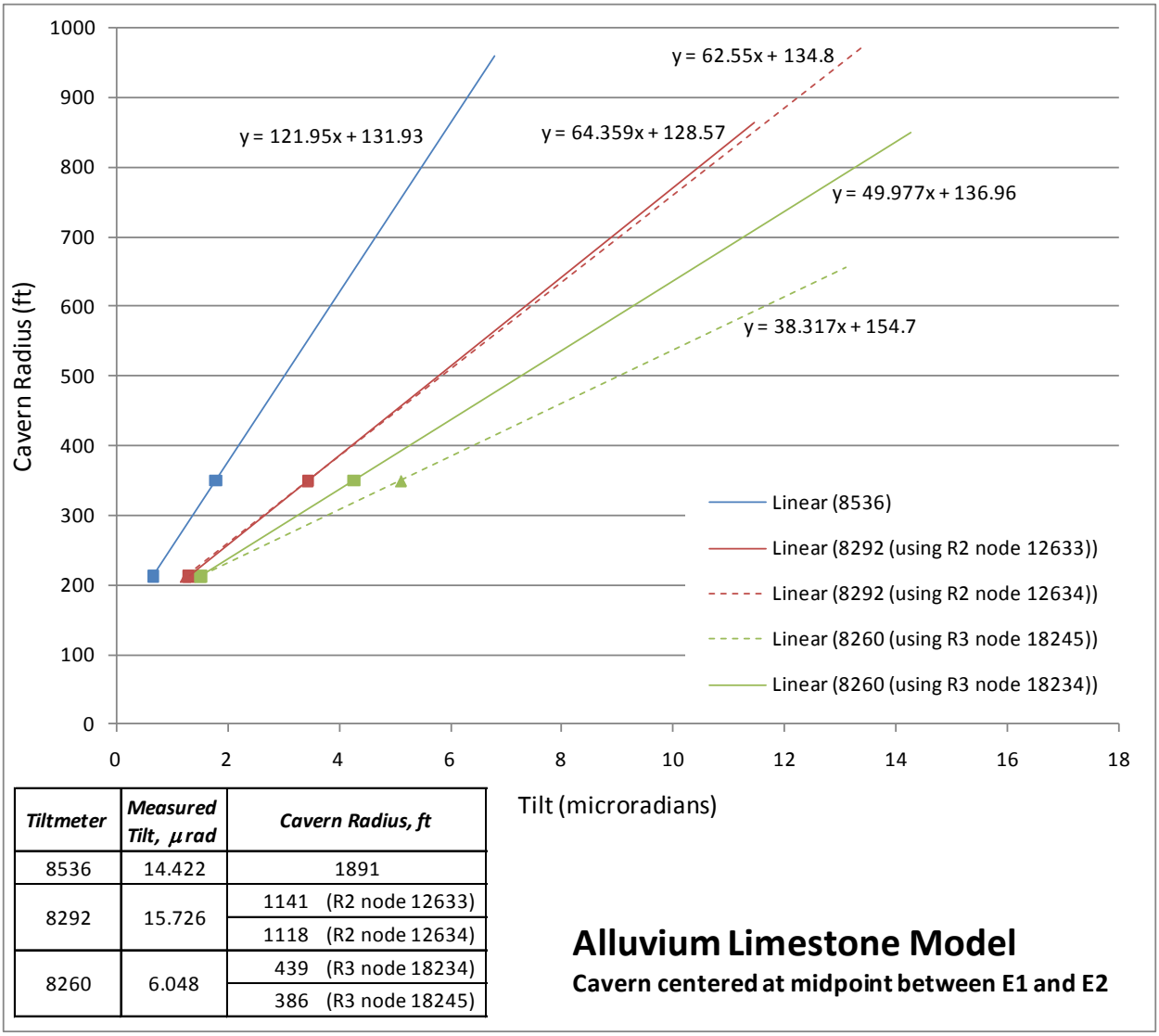

Tiltmeter	*Measured Tilt, µrad*	*Cavern Radius, ft*
8536	14.422	1891
8292	15.726	1141 (R2 node 12633)
		1118 (R2 node 12634)
8260	6.048	439 (R3 node 18234)
		386 (R3 node 18245)

Figure 23. Linear extrapolation of the predicted maximum changes in tilt over the 22 hr period of cavern bleed off for R2 and R3 cavern sizes in models where the alluvium is modeled as a weak limestone. The cavern is assumed to be centered at the midpoint between Eugenie 1 and 2. The inset table lists the circular cavern radius that would be required to produce the observed tilt changes at the specific tiltmeter.

Figure 24 and 25 show the results of the logarithmic extrapolation of the numerical results. Figure 24 is for the case where the alluvium is modeled as a sand and gravel soil; Figure 25 is for the case where the alluvium is modeled as a weak limestone. For a specific tiltmeter, the curve through the numerically predicted data is extended until the maximum observed change in tilt for that tiltmeter is reached. This produces estimates of a circular cavern radius necessary to produce the observed tilt changes. The tables inset in the plots indicate the results. In general the required cavern sizes required to obtain the field data for the logarithmic extrapolations are much smaller than for the linear extrapolations. The observed tilt changes for Tiltmeter 8536 require the largest cavern radii: 550 ft for the soil alluvium model and 640 ft for the weak limestone alluvium model. The difference is attributed to the higher stiffness that the limestone model has which requires a larger cavern radius to obtain the same change in tilt. The field data for Tiltmeter 8292 required the next largest cavern diameters. For the soil model, a cavern radius of 470 ft would be required; and for the limestone model, a cavern radius of about 560 ft (using the average of the nodal predictions) is needed to obtain the observed deformation. The data for Tiltmeter 8260 matched the observed data fairly well for the R3-size cavern (Figures 20 and 21), so the extrapolated results do not suggest a differently sized cavern.

Even though it seems that the cavern should be centered about the midpoint between Eugenie 1 and Eugenie 2 based on the age of the facility, we can use the data from the cavern being centered around Eugenie 1 to get an idea about which fit trend line is more realistic since we would have three data points. The results of this exercise are shown in Figures 26 and 27. It can be seen that the logarithmic fit is a much better choice. In addition, if the cavern is centered around Eugenie 1, the inset tables on Figures 26 and 27 show the extrapolated sizes of caverns which would be needed to match the measured field data. The extrapolated sizes of the caverns in Figures 26 and 27 are smaller than those for the caverns being centered at the midpoint between Eugenie 1 and 2. The largest extrapolated cavern size for the alluvium being modeled as a sand and gravel soil is 430 ft in radius, and for the alluvium being modeled as a weak limestone the cavern would need to be 450 ft.

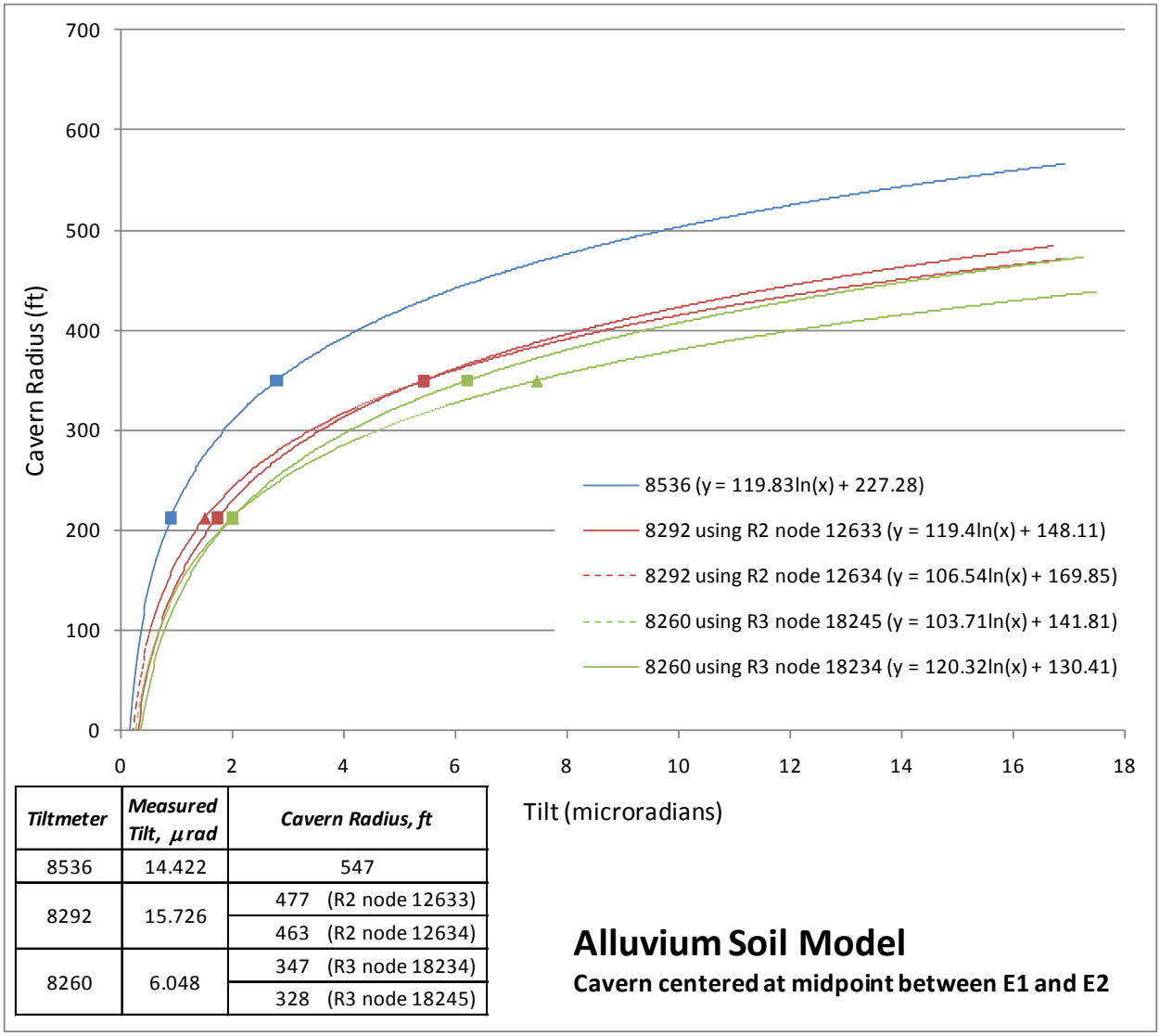

Tiltmeter	*Measured Tilt, µrad*	*Cavern Radius, ft*
8536	14.422	547
8292	15.726	477 (R2 node 12633)
		463 (R2 node 12634)
8260	6.048	347 (R3 node 18234)
		328 (R3 node 18245)

Figure 24. Logarithmic extrapolation of the predicted maximum changes in tilt over the 22 hr period of cavern bleed off for R2 and R3 cavern sizes in models where the alluvium is modeled as a sand and gravel soil. The cavern is assumed to be centered at the midpoint between Eugenie 1 and 2. The inset table lists the circular cavern radius that would be required to produce the observed tilt changes at the specific tiltmeter.

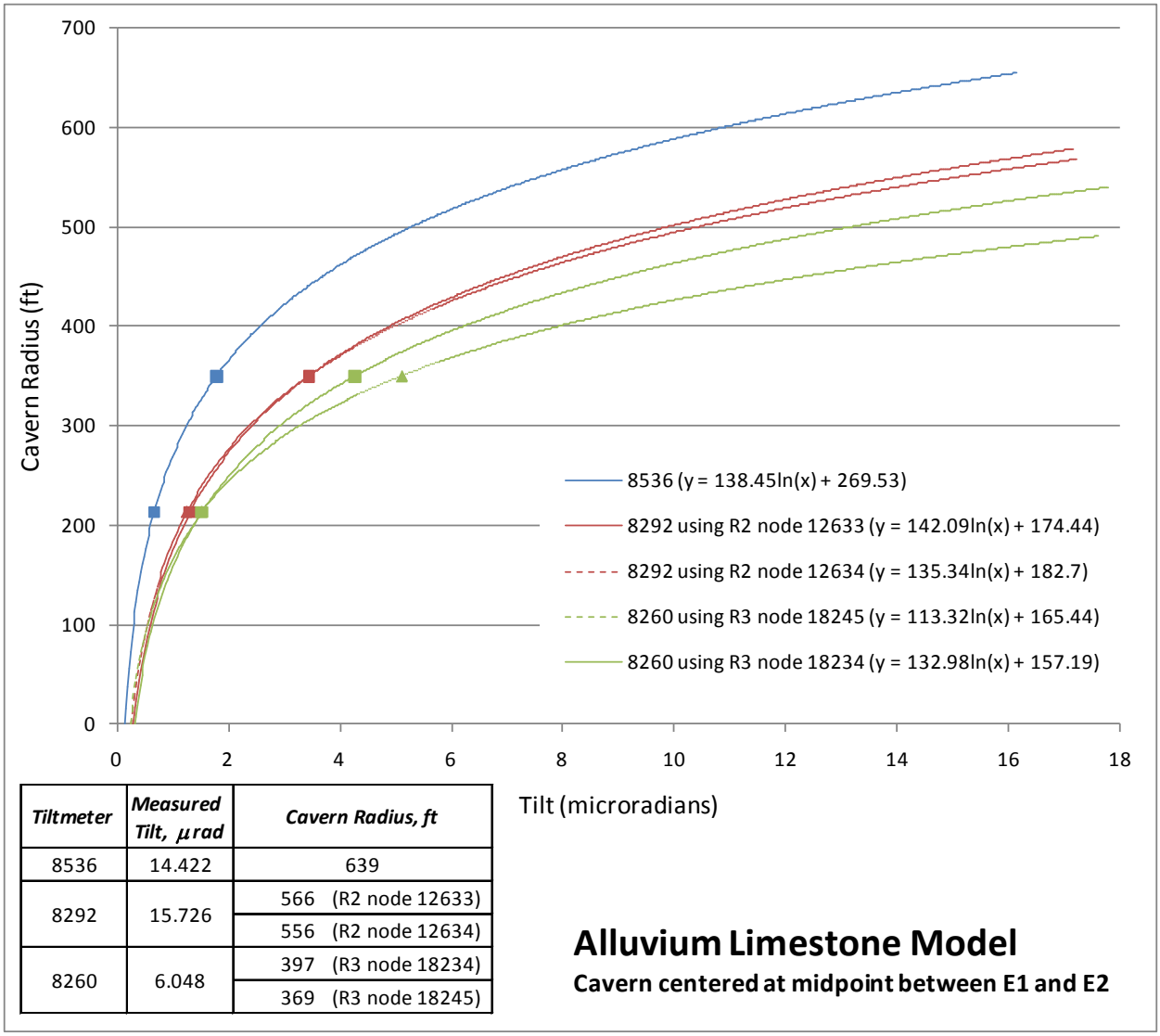

Tiltmeter	*Measured Tilt, µrad*	*Cavern Radius, ft*
8536	14.422	639
8292	15.726	566 (R2 node 12633)
		556 (R2 node 12634)
8260	6.048	397 (R3 node 18234)
		369 (R3 node 18245)

Figure 25. Logarithmic extrapolation of the predicted maximum changes in tilt over the 22 hr period of cavern bleed off for R2 and R3 cavern sizes in models where the alluvium is modeled as a weak limestone. The cavern is assumed to be centered at the midpoint between Eugenie 1 and 2. The inset table lists the circular cavern radius that would be required to produce the observed tilt changes at the specific tiltmeter.

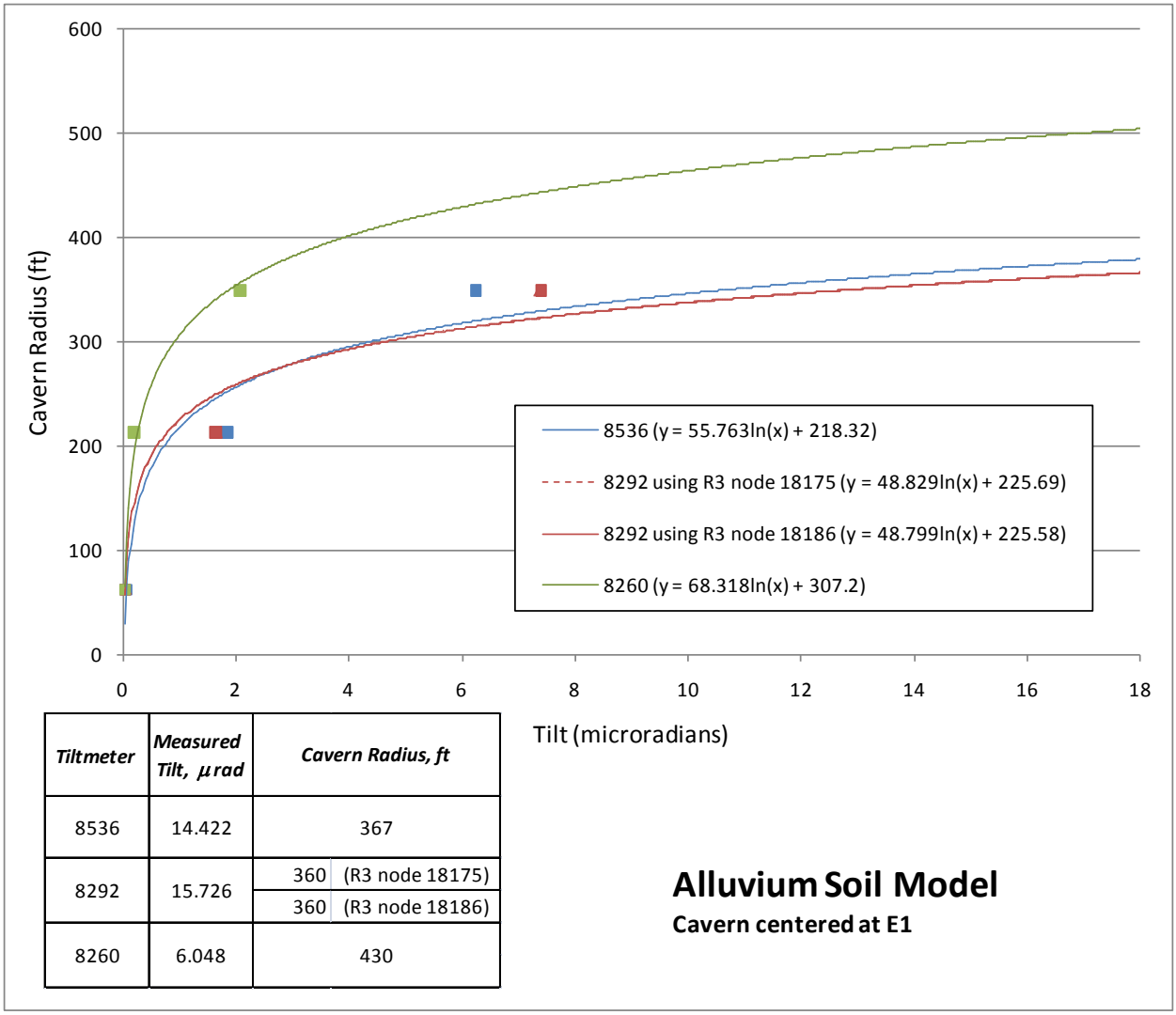

Tiltmeter	*Measured Tilt, µrad*	*Cavern Radius, ft*
8536	14.422	367
8292	15.726	360 (R3 node 18175)
		360 (R3 node 18186)
8260	6.048	430

Figure 26. Logarithmic extrapolation of the predicted maximum changes in tilt over the 22 hr period of cavern bleed off for all cavern sizes in models where the alluvium is modeled as a sand and gravel soil. The cavern is assumed to be centered around Eugenie 1. The inset table lists the circular cavern radius that would be required to produce the observed tilt changes at the specific tiltmeter.

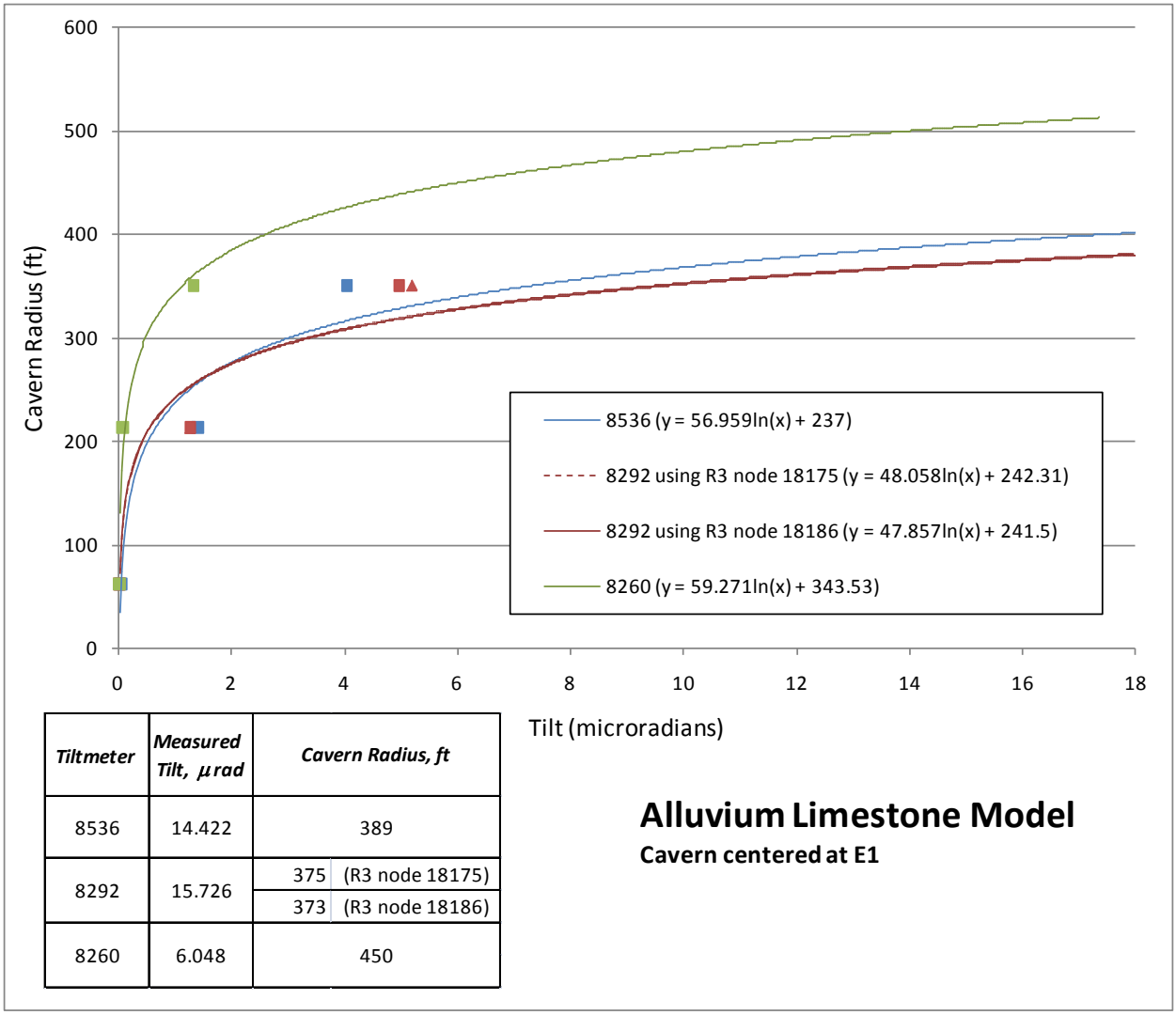

Tiltmeter	*Measured Tilt, μrad*	*Cavern Radius, ft*
8536	14.422	389
8292	15.726	375 (R3 node 18175)
		373 (R3 node 18186)
8260	6.048	450

Figure 27. Logarithmic extrapolation of the predicted maximum changes in tilt over the 22 hr period of cavern bleed off for all cavern sizes in models where the alluvium is modeled as a weak limestone. The cavern is assumed to be centered around Eugenie 1. The inset table lists the circular cavern radius that would be required to produce the observed tilt changes at the specific tiltmeter.

4 Conclusions and Recommendations

In July 2010, the brine cavity at the I&W brine well site in Carlsbad, New Mexico was depressurized by allowing the cavity to flow out over a 22-hour period. This action resulted in a significant ground response from the three borehole tiltmeters located near the surface above the cavity, with an increase in tilt at each monitoring location. The overall size and extent of the I&W cavity is unknown. In an effort to characterize the I&W cavity, a finite element analysis using a simplified mesh to model the I&W site was developed to evaluate the response of the rock mass above the solution-mined cavern.

Three different sizes of cylindrical cavities in the salt layer were used to simulate the actual cavern. The first cavern size (R1) is the average horizontal size of the upper cavern at Eugenie 1, the second cavern size (R2) is equal to the equal to the horizontal area interpreted as showing some seismic effect (Goodman et al., 2009), and the last (R3) was of a large cavern that when centered at Eugenie 1 extended beyond Eugenie 2. It seemed large enough to capture the entire area showing any seismic effects, including early interpretations which were slightly larger than the present interpretation.

The finite element model was developed to simulate the events of the first re-entry attempt through Eugenie 1. During that event, the upper Eugenie 1 cavern was entered at a wellhead pressure of 30 psi. The cavern was allowed to bleed off for about 22 hours. The final wellhead pressure was 14 psi. For purposes of the numerical simulation, the pressure in the cavern corresponding to the surface wellhead pressure was dropped in a linear fashion for the duration of the bleed off. This does not quite mimic the actual situation where the brine flow rate was increased from 1 bbl/min to 3 bbl/min for the last hour of the re-entry attempt. For the material properties chosen for the two overlying layers, the change in flow rate should not affect their response.

The range of modeled cavern radii was not sufficient to capture the changes in tilts recorded by the three tiltmeters that were at the I&W site at the time of the re-entry. In many cases, the numerically simulated tilts were less than half the observed actual data. Since the field changes in tilt are larger than the numerically derived changes in tilt, the actual cavern must be larger than the modeled caverns.

A couple attempts to extrapolate the simulated tilt results to match the field data were made. The first involved a linear fit and the second involved a logarithmic fit to the R2 and R3 sized cavern data because it is believed that, due to the age of the facility, the more likely center of the cavern would be at the midpoint of Eugenie 1 and 2 (personal communication with John Plosz and Peter Jackson, The Mosaic Company). With only two data points to fit the data to, there is a large amount of uncertainty associated with any predictions. The linear model extrapolation predicted the largest cavern sizes, ranging from radii of 330 ft to 1900 ft depending on the tiltmeter being investigated and the material parameters chosen for the alluvium. The logarithmic extrapolation predicted cavern radii of 330 ft to 640 ft for caverns centered at the midpoint between the injection and production wells (Eugenie 2 and 1, respectively). If we assume that the cavern center is around Eugenie 1, a better trend for the data is obtained. It is seen that a logarithmic fit is better than a linear fit. The logarithmic extrapolation predicted cavern radii of 360 ft to 450 ft for caverns centered around Eugenie 1.

As for recommendations, the present modeling could be made more sophisticated and appropriate in a number of ways. Some simple suggestions include:

- More models using larger cavern radii are required to obtain a better constraint on the possible cavern size. This includes not only reproducing the measured field tilt changes, but

also in fitting an extrapolation or interpolation. The range of cavern sizes used herein was insufficient.

- The predicted cavern sizes are dependent on the properties chosen for the overlying layers. The most questionable layer model is for the alluvium since parameters for the Rustler have apparently been obtained from past studies. The proposed drilling of additional boreholes with accurate borehole logging and collection of data pertaining to the rock physical properties will be quite valuable.

- The location of the cavern has not been determined. Moving the modeled cavern around may help optimize the differences between the measured and predicted changes in tilt. Time was not taken to analyze the tilt directions measured at the site during this re-entry attempt.

- Shapes other than a cylinder could be investigated also. Some of the reasoning in using a quadrant mesh rather than an axisymmetric mesh was that different shapes, i.e. an oval shape, would be possible to include in future analyses. It is also possible to incorporate cone shaped caverns, but their effect on modeling the re-entry data should be small.

5 References

Argüello, J.G., J.E. Bean, C.M. Stone, and B.L. Ehgartner. (2009) Geomechanical Analyses to Investigate Wellbore/Mine Interactions in the Potash Enclave of Southeastern New Mexico. Sandia Report SAND2009-4795. Albuquerque, New Mexico.

Bachman, G.O. (1974) Geologic Processes and Cenozoic History Related to Salt Dissolution in Southeastern New Mexico. USGS Open-file Report 74-194

Blanford, M. L. (2001) JAS3D – A Multi-Strategy Iterative Code for Solid Mechanics Analysis: User's Instructions, Release 2.0. Sandia National Laboratories, Albuquerque, New Mexico.

Caltrans. (2003) Bridge Design Specifications, Section 4 – Foundations. California Department of Transportation, Sacramento, CA.
http://www.dot.ca.gov/hq/esc/techpubs/manual/bridgemanuals/bridge-design-specifications/bds.html

Das, B.M. (2006) Principles of Geotechnical Engineering, 6th ed. Nelson, Ontario, Canada.

Goodman, W.M., J.M. Schneider, D.J. Gnage, D.A. Henard, and L.L. Van Sambeek. (2009) Two-Dimensional Seismic Evaluation of the I&W Cavern, Carlsbad, New Mexico. RESPEC Topical Report RSI-2083. Prepared for New Mexico Oil Conservation Division. Rapid City, South Dakota.

Holtz, R.D. and W.D. Kovacs. (1981) An Introduction to Geotechnical Engineering. Prentice Hall, Upper Saddle River, NJ.

Henard, D.A., L.L. Van Sambeek, M.G. Wallace, W.M. Goodman, C.M. Hocking, C.A. Barber, E.L. Krantz. (2009) Geohydrological and Structural Analysis and Monitoring I&W Cavern, Carlsbad, New Mexico: Status Report No. 1. RESPEC Topical Report RSI-2060, Revision 1. Prepared for New Mexico Oil Conservation Division. Rapid City, South Dakota.

Hendrickson, G.E. and R.S. Jones. (1952). Geology and Ground-Water Resources of Eddy County, New Mexico. Ground-Water Report 3. New Mexico Bureau of Mines & Mineral Resources, a division of New Mexico Institute of Mining & Technology. Socorro, New Mexico

Munson, D.E. and P.R. Dawson. (1979) Constitutive Model for the Low Temperature Creep of Salt (with Application to WIPP). Sandia Report SAND79-1853. Albuquerque, New Mexico.

Munson, D.E. and P.R. Dawson. (1982) A Transient Creep Model for Salt during Stress Loading and Unloading. Sandia Report SAND82-0962. Albuquerque, New Mexico.

Munson, D.E. and P.R. Dawson. (1984) Salt Constitutive Modeling Using Mechanism Maps. The Mechanical Behavior of Salt, Proceedings of the First Conference. Pennsylvania State University, University Park, PA. November 9-11, 1981. Eds. H.R. Hardy, Jr. and M. Langer. Karl Distributors, Rockport, Massachusetts. pp. 717-737.

Munson, D.E., A.F. Fossum, and P.E. Senseny. (1989) Advances in Resolution of Discrepancies between Predicted and Measured, In Situ Room Closures. Sandia Report SAND88-2948. Albuquerque, New Mexico.

Palchik, V. (2010) On the Ratios between Elastic Modulus and Uniaxial Compressive Strength of Heterogeneous Carbonate Rocks. Technical Note. Rock Mechanics and Rock Engineering DOI: 10.1007/s00603-010-0112-7. http://dx.doi.org/10.1007/s00603-010-0112-7.

SOCON. (2010) Echo - Log City of Carlsbad Eugene #1: Carlsbad, New Mexico 09/09/2010. Report 103049. SOCON Sonar Well Services, Inc. Conroe, Texas.

USACE (US Army Corps of Engineers). (1990) Engineering and Design – Settlement Analysis. Engineer Manual (EM) 1110-1-1904. Table D-3, p. D-5. Dept. of the Army, Washington, DC. http://140.194.76.129/publications/eng-manuals/em1110-1-1904/toc.htm

Van Sambeek, L.L. (2010) Summary of Eugenie #1 Reentry, Former I&W Facility, Carlsbad, NM. July 13 presentation to the City of Carlsbad Technical Committee.

Sandia National Laboratories is a multi-program laboratory managed and operated by Sandia Corporation, a wholly owned subsidiary of Lockheed Martin Corporation, for the U.S. Department of Energy's National Nuclear Security Administration under contract DE-AC04-94AL85000.